ISTITUTO NAZIONALE DI FISICA NUCLEARE

Sezione di Genova

INFN/code-00/001
23 Luglio 2001

INDIRECTLY COOLED SUPERCONDUCTING DIPOLE FOR A ION GANTRY

M. Conte[1,2], P. Fabbricatore[2], S. Farinon[2], F. Gerardi[3], R. A. Laurenti[4], R. Musenich[2], P. Negri[3], M. Perrella[4], C. Priano[3], S. Rebora[2,5], L. Reina[5], S. Rossi[3], S. Squarcia[1,2], P. Zadaricchio[1]

[1)]Dipartimento di Fisica - Universitá di Genova, Via Dodecaneso 33,I-16146 Genova, Italy
[2)]INFN - Sezione di Genova, Via Dodecaneso 33, I-16146 Genova, Italy
[3)]Fondazione TERA, Via Puccini 11, I-28100 Novara, Italy
[4)]ANSALDO Superconduttori s.p.a., Corso Perrone 25, I-16121 Genova, Italy
[5)]Dipartimento di Meccanica e Costruzione delle Macchine - Universitá di Genova, Via all'Opera Pia 15 A, I-16145 Genova, Italy

Abstract

We present the ATER/TESI intermediate status report on a superconducting ion gantry usable in advanced techniques of tumour radiotherapy. Ions application for the cure of radio resistant tumours is becoming more and more important and, in order to optimise the distribution of dose, the possibility of rotating the magnet around the patient is fundamental. While for proton gantry projects different solutions exist, gantries for ions are still in phase of plan and the single one that appears to be the nearest to the operational phase has been carried out by the GSI of Damstadt. The study of the conductor characteristics, the dipole shape, the 2D flux lines and the magnetic field map, with an uniformity better of 1‰ in the interesting zone, the preliminary 3D simulation and the beam tracking inside the magnet is presented with the dipole bending machine drawings and the cryogenic layout discussion.

*Published by **SIS–Pubblicazioni***
Laboratori Nazionali di Frascati

1. INTRODUCTION

Heavy particles (up to Ne ions) are one of the more recent and promising method used in tumor therapy for specific well localized cancer. The general goal of any radiotherapy irradiation technique is to conform the dose to the target volume sparing as possible organs at risk. This goal is achieved by radiation with high physical and biological selectivity and using a multi-field 3D-conformal irradiation technique. For proton and ion therapy beams, this means delivering the beams with the aid of a rotating structure, called "gantry" that, in a similar way of all the conventional radiotherapy structure, allows to select the best directions to hit the target volume. Moreover the gantry should be equipped with an active scanning system. Otherwise, unique favorable physical and biological properties of light ions could not be fully exploited.

Constructing an ion gantry brings serious technical difficulties if considering the conventional technology. Because of high magnetic rigidity of ion therapy beams (over 6 Tm), dictated by desirable penetration range of ions in the patient body (around 25 cm) that require an energy of 4.5 GeV of carbon ions, the gantry weight and dimensions exceed some practical limits, especially when considering a dedicated installation in a common hospital environment.[1)]

There are three proposals[2),3),4)] for gantries equipped with superconducting magnets, but no detailed design-study is available in these proposals. A system has been proposed[5)] where rapid energy changes can be carried out, still using SC magnets, by compensating the radius variations via conventional magnets. It is worthwhile to underline that, as regards to the use of ions in hadrontherapy, neither normal nor superconducting gantries has been built so far. The possibility of using a superconducting technology with a cryo-cooler has been studied as an interesting option for the ion gantry. In this report we present the results obtained so far in:

1. Design of the general project "superconducting gantry" environment.
2. Preliminary design of the beam transport system.
3. Design of the magnet system.
4. Winding layout and techniques.
5. Magnet 3D optimization.
6. Cryogenic layout.

We are confident this project can arrive, in few years time, to a final industrial project.

2. HADRON THERAPY AND THE RATIONALE BEHIND

Charged hadrons differ considerably from electrons and photons (used today in conventional radiotherapy) in that they penetrate matter with minimal scattering and deposit the maximum energy density in a 'peak' at the end of their range, just before coming to rest. To treat a tumour, the so-called 'Bragg peak' should be placed only in the tumour, which is scanned longitudinally by varying the range (i.e. the energy) of the incident hadrons. To penetrate 26 cm in the body of a patient, protons (i.e. Hydrogen atoms stripped from their electrons to become ions) have to be accelerated to a kinetic energy of 200 MeV and fully stripped Carbon ions have to reach about 4500 MeV (i.e. 380 MeV/u). These energies are much larger than the ones needed for therapeutic Bremsstrahlung production (up to 50 MeV peak energy), based on electron accelerators that are at present the standard instruments in radiotherapy departments. Since hadrons are much heavier than electrons (2000 times and more), the acceleration systems needed for hadron therapy are much larger and more costly than the ones used in hospitals today.

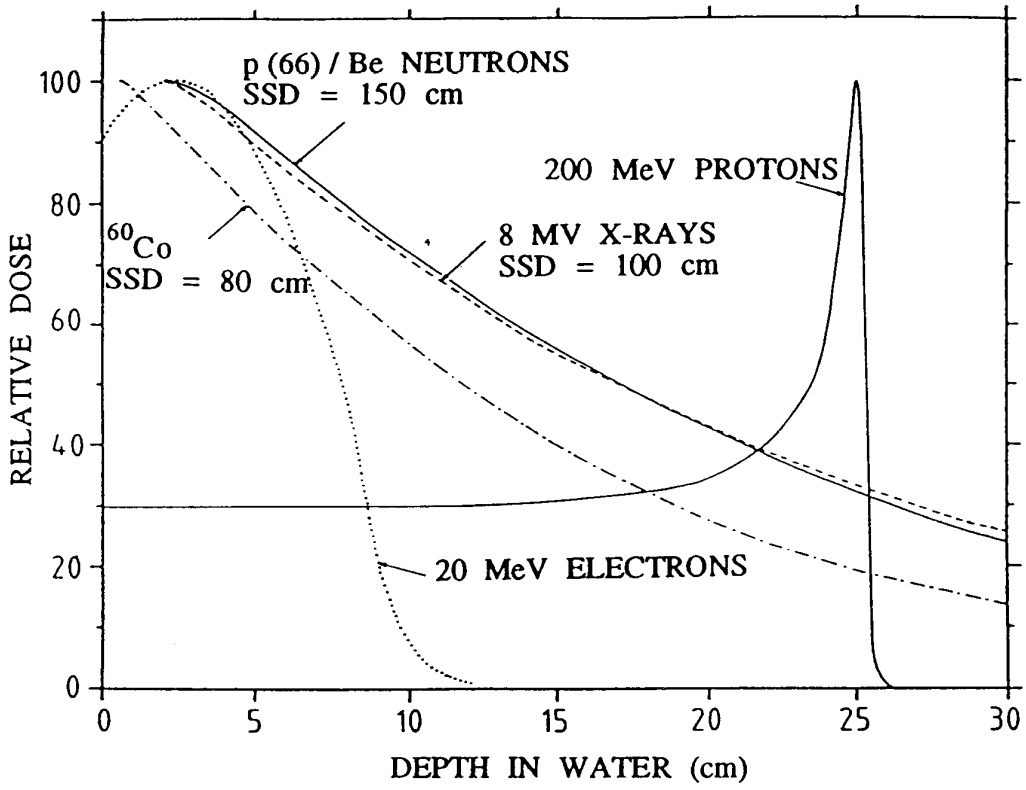

FIG. 1: Depth dose distribution for different type of radiation and particles used in radiotherapy.

TAB. I: Clinical requirements on the therapeutic beam.

Beam range in water	1.0 g/cm^2 to 26 g/cm^2
Bragg peak modulation Range adjustment Treatment time at 1 - 1.5 Gy in one litre	< 2.5 mm < 2.5 mm (1σ) < 1 min
Field size	Horizontal beams: 40×32 cm^2 Gantries and vertical beams: 20×20 cm^2
Pencil beam FWHM adjustable	4 – 10 mm
Field size adjustment	1 mm steps
Field size accuracy	± 0.5 mm
Field uniformity (lateral)	< 2%
Field uniformity (longitudinal)	< 2%
Field symmetry	< 2%
Lateral penumbra (80 – 20 %)	< 1.5 mm more than the multiple scattering contribution
Distal dose fall-off (80 – 20 %)	< 2 mm in addition to intrinsic distal fall-off in uniform media

Tab. I summarises the specifications proposed for the clinical hadron beams. Most of them are either similar or more stringent than those used by existing and planned particle therapy centres and conventional treatment units using electron and photon beams.

Protons, and in particular light ions, are ideal for intensity modulated treatments because of *three physical properties*. Firstly, they penetrate the patient practically without diffusion. Secondly, they deposit their maximum energy density abruptly at the end of their range, where they can produce severe damage to tumour cells while sparing both traversed and deeper located healthy tissues. Thirdly, being charged and accelerated by a synchrotron they can easily be formed as narrow focused and scanned pencil beams of variable penetration depth so that any part of the tumour can be accurately and rapidly irradiated. Thus, a beam of protons, or light ions, allows a real 3D conformal treatment of deep-seated tumours with millimetre accuracy in the tumour, giving minimal doses to the surrounding tissues.

The superconducting dipole described in this page will be implemented in vertical lines and gantries, so that the field size that has to be guaranteed by the treatment modality is

200×200 mm^2. The good field region of the superconducting bending dipole has been fixed to 200×60 mm^2. The horizontal dimension (200 mm) coincides with the dimension of the field size specified in Tab. I, the vertical aperture is minimized to reduce the impact on the dipole design characteristics. This size is nevertheless larger than the beam minimum size, to take into account misalignments and errors, and to allow a smoothing of the dose profile for each mini-slice. This choice of the good field region is strictly related to the active scanning system foreseen to cover the field size. It is foreseen to scan the beam along the median plane of the dipole and to move the patient in the other orthogonal transverse direction. The patient displacement is the slowest movement in the scanning system. The depth in the patient of the delivery dose can be varied by changing the extraction energy from the synchrotron or inserting a passive degrader just in front of the patient. The adoption of the energy variation at the extraction implies a field variation in the superconducting dipole that that is at present under study; the passive degrader introduces an increase in the fragmentation tail of the SOBP that has to be carefully estimated.

To date about 30˙000 patients worldwide have undergone *proton therapy* and very good results have been obtained in head and neck cancers. Indications on proton therapy and clinical results can be found in two review articles.[6),7)] Most of these patients have been treated in nuclear research centres by using a single hadron beam often with sub optimal characteristics. To really use hadron therapy in the clinic, hospital based centres with multiple treatment rooms running with an uptime of 96% are needed. Two proton therapy centres of this type are at present running in the world: the Loma Linda University Medical Centre in USA and the Kashiwa Cancer Centre in Japan. Moreover Carbon ions are used since 1994 at HIMAC (Chiba, Japan) and since 1997 at GSI (Darmstadt, Germany). One new ion centre (Hyogo, Japan) and two proton centres (Mass. Gen. Hospital, Boston, USA and Tsukuba, Japan) will treat their first patients in the year 2001. Finally two other hospital based proton therapy centres are being built in Japan. All these centres are described in Ref. [8]. At present, there exist no centre in the world with rotating gantry for ions; various projects have been proposed,[9),10)] but with dimensions, weights and power consumptions of the gantry often exceedingly high. In fig. 2 is shown the layout of the gantry proposed for the GSI facility, the last dipole bends the beam by 90° with a maximum field of 2 T, the total weight of the gantry is of 675 t.

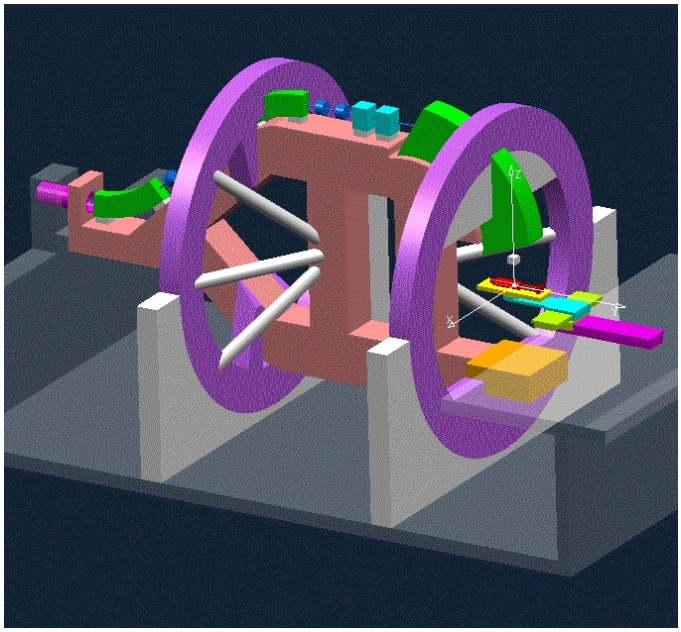

FIG. 2: Scheme of the GSI isocentric gantry [www.gsi.de].

Some of these projects are based on an innovative design called "Riesenrad"[11] that uses a 90° bending dipole placed on the rotation axis with the patient placed in a mobile cabin that rotates on a circle around it. This solution with the patient movement along a circumference with diameter of at least 3 m, is accepted very likely by the physicians, because the patient is not readily and easily reached in case of problems and emergencies.

3. BEAM OPTICS

The requirements made in the former section dictate an extremely careful design of the "magnetic channel" that brings the particles from the synchrotron to the patient. To obtain the shortest (and cheaper) beam line was chosen to combine the different required module[11] instead of having separate beam line section for the various control function of the beam characteristic at the isocentre. For this reason the design of the optics of the gantry cannot be done without the design of the previous beam line section starting from the extraction septum in the synchrotron. A possible layout of this beam line, considered in this case as fixed vertical beam line and not as rotating gantry, is illustrated in fig. 3, where the beam is raised by a couple of bending magnets, often called dipoles, until about 5.7 in height, then is bent to become horizontal again and finally is turned down by a 90° bending system until the isocenter. The high of the beam pipe respect to the isocentre (that can be seen as the minimum radius of the isocentric gantry) is strictly connected to the last dipole radius because other equipment fixes the distance from the dipole edge and the isocentre. Hence from fig. 3 can be easily shown that a decrease of the last dipole radius brings to a smaller gantry.

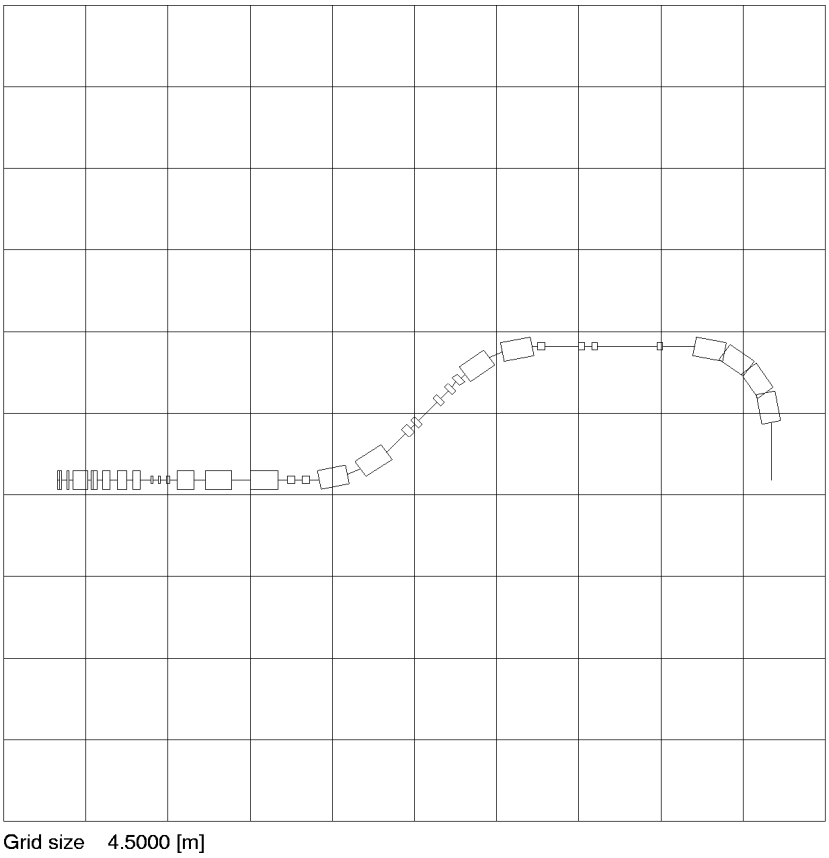

FIG. 3: Beam line layout, side view.

The SC dipole presented in this study is foreseen only as last dipole while all the other bending magnets required in the beam line are normal conducting magnets and in this case equal to the dipoles of the synchrotron,[11] reducing in this way their cost. The last dipole (longer, bigger and heavier) should be replaced by a SC magnet reducing the size and weight. The optics design was afforded using the WinAGILE[12] program that allows describing by computer simulation the characteristics of the beam line, succeeding in visualizing in each point the beam properties, such as dimensions, divergences, energy spread and phase spaces distribution. This program allows the user to represent the beam line in a very detailed description. It also contains a powerful matching function that helps us to find the correct set of parameters assigning variables and constraints along the beam line. The first thing to do is to verify the beam size on the patient, which, following the clinical requirement, must have a FWHM from 4 to 10 mm. This study leads us towards a peculiar aspect of the beam due to the process of slow extraction from the synchrotron. If we take a look at the beam distribution in the horizontal phase space, i.e. that

representative plane where the co-ordinates are respectively the horizontal displacement x of a single particle from the ideal orbit and the horizontal slope x' of its trajectory, we see in the extraction plane a thin rectangle called the bar of charge.[11] An example of this bar is shown in fig. 4, together with the corresponding representation in the vertical space plane, i.e. that representative plane whose coordinates are the vertical displacement z and the vertical slope z' of the beam particles. Such a situation determines a particular approach in the size study; instead of working on the beta functions β_H and β_V which refer respectively to the horizontal and vertical betatron oscillations, as it is done in more *usual* situation because the square roots of such beta functions are proportional to the beam dimensions, for the horizontal beam size study it is preferable to control how this bar rotates in the phase plane, since its projection on the x-axis determines the size of the beam.

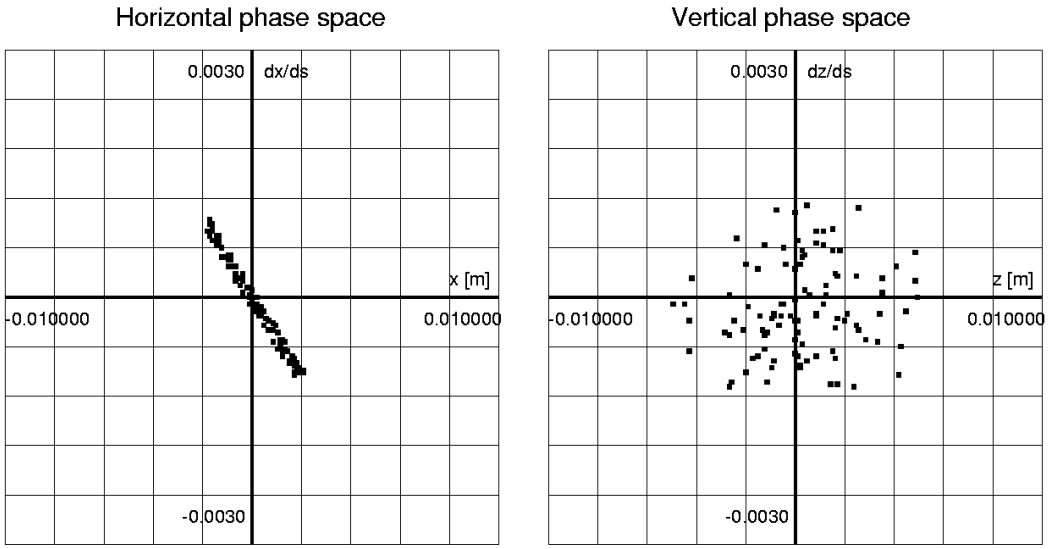

FIG. 4: Example of bar of charge.

On the patient there are other conditions to be fulfilled: the displacement depending on the energy spread has to be minimized, i.e. the dispersion function must be zero, and the beam dimensions have to be kept constant while crossing the tumor, i.e. the so called α Courant-Snyder functions are equal to zero. Anyway it is true that the beam study is not limited at the final position, its evolution must be controlled in every single point along the beam line, to avoid anomalous situations such as excessive beam size that would lead to particles losses during the transfer.

We started from the extraction line designed by CNAO; in our work we have preferred not to modify the first part of this program, because it deals with other branches to be inserted beyond the gantry we are studying. The portion of line under consideration is constituted of bending dipoles, drift sections and quadrupoles. The last dipole is still rather different from the superconducting magnet we are planning to build; this is due to a WinAGILE limitation, which permits the user to work only on ideal magnets, thus a very realistic design of such a particular dipole results rather difficult. However the beam information till this last element appear to be accurate and appropriate for a separate study of the optics inside the magnet that track in a detailed way each particle in the real magnetic field. The variables used are the quadrupole strengths, which are expressed via the parameter $k = q \cdot G/p$, where q is the ion charge, G is the gradient of the magnetic field inside the quadrupole, and p is the particle momentum. Values of k varying from $-3.2 m^{-2}$ to $+3.2 m^{-2}$ have been considered so far. The solution produced by the automatic matching procedure must be checked very carefully because the code cannot take into account some real aspects. First of all the drift sections cannot become shorter than 30 cm: quadrupoles assembling and their coils need a certain amount of space; then the drift length between the last dipole and the isocenter, where the patient is placed, has to be of the order of 2÷3 m, to be finally assessed depending upon refinements and possible additions. With this aim the length of the ascending stretch, or ramp, of the beam line must be checked very carefully, because it determines the position with respect to the patient of the last dipole, if the bending angles of the other dipoles are kept unvaried. Since a scanning magnet has to be inserted, it is necessary to assure a free space in the line where it will be assembled: this involves a further limitation in elements positioning.

At present, the simulation program is working on 9 quadrupoles (5 on the ramp and 4 on the following horizontal section), the variables are the k values (by which we control the quadrupoles strength) with the limits mentioned above and the positions of some of them, while the other variables have been already fixed due to the motivations discussed before. Additional constraints are to be imposed along the machine to keep as small as possible the magnitudes of β_H, β_V and of the dispersion functions, the latter being those parameters which account for how the beam size depends upon the energy spread. Till now gantry rotations have not been simulated, this implies changes in beam optics, that must be taken into account.

4. DESIGN GUIDELINES

One of the basic requirements for a superconducting bending dipole for the gantry is that *the cooling system shall not involve the use of cryogenic liquids (namely LHe, i.e. liquid helium), due to the negative impact on medical environment (for the complexity of the operations).* As a result we chose to cool the winding with a cryo-cooler, which can be operated in very simple way. Nevertheless the impact on the dipole design is quite strong:

- Due to relatively low available cooling power at 4.5 K (3 W), we have to design a superconducting winding based on the criterion of *indirect cooling*. This means that, the cooling system shall be able to remove the limited heat loads (due to cryostat heat loss and to current leads), but it shall not be able to protect the winding from thermal disturbances. Local energy releases for mechanical or electrical reason shall be recovered by the winding itself. This is not a new idea, the coils used in the detector for HEP are based on this criterion. In order to survive from localized disturbances, the superconducting cable is immersed in a pure aluminum matrix, which also limits the temperature rise in case of quench.
- On the other hand, we have dissipation inside the coil, when the field is ramped up/down during a therapy cycle. We have to keep the current density in the aluminum matrix as low as the total temperature increase is within the limit. At the same time the superconducting cable is designed with the aim to minimize the heat dissipation during field variations; so we have fine filaments (<10 μm), small twist pitch and barriers limiting the transverse current (not yet implemented in the present design). As superconducting material we chose NbTi, because, though the relatively low critical temperature (9.2 K), it is the most known material involved in superconducting magnet (Nb_3Sn is too brittle for bent dipoles, high T_c are not yet developed at industrial level).
- Current leads are sources of dissipation. The maximum current is then set to 1 kA. This is also the minimum current in order to limit the number of turns and then the coil inductance, which plays an important role in case of quench.
- The field uniformity required in the large space, in which the ion beam can move, requires a special winding layout. The use of several bent racetracks allows having a number of geometrical parameters for a field optimization.
- Since the winding is made of aluminum stabilized conductor, it is highly recommended to involve aluminum in the mechanical structure. In this case we can

have a containing structure with good thermal properties (an advantage for the cooling) and same thermal contraction (this limits the mechanical stress). Of course the aluminum shall be a suitable alloy, with excellent mechanical properties (high yield and tensile stress, good elongation).

The abovementioned points constitute the basic guidelines, around which the design was performed.

5. WINDING 2D LAYOUT

The goal of this work is then to design a superconducting dipole able to generate a magnetic field of 4 T along a circular path, 1.6 m in radius and 90° angularly. The field uniformity in a region of rectangular section 200×60 mm^2, describing the beam path and centered at r=1.6 m, should be better than 2‰. Such a magnet has to be composed by a certain number of bent racetrack coils, shaped as shown in fig. 5.

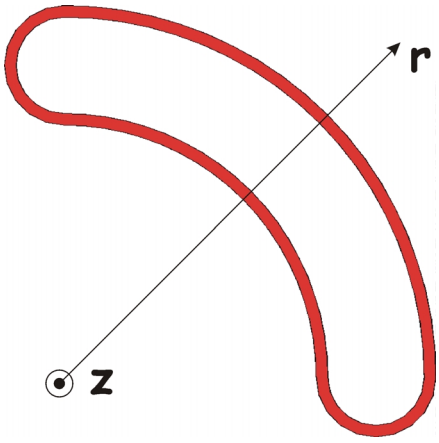

FIG. 5: Shape of the bent racetrack coils composing the dipole.

A preliminary analysis allowed us to define the overall shape of the superconducting magnet, shown in fig. 6: the coil on the equatorial plane was split into two independent coils, in order not to occlude the path to the ion beam, and the total number of bent racetrack coils was fixed to 10, symmetric with respect to the equatorial plane. Subsequently, an exhaustive optimization analysis was carried out, in order to define completely the magnetic design of the superconducting dipole. The starting point of that analysis was the identification of all the constraints that tie the design (described in the following paragraph); then the final optimization, performed using Finite Element analyses driven by a genetic algorithm, led to a best design which fulfills all the project requirements.

The magnetic optimization analysis was performed in two steps. Considering that the magnetic field in the center of the dipole should not be greatly influenced by the behavior of the two ends, the first step consists in 2D axis-symmetric analysis performed on a section sufficiently far from the coil heads (see fig. 7). The aim of that analysis is to maximize the field uniformity in the region 200×60 mm^2, keeping into account all the

design requirements listed in §5.1. A second step was then performed, shaping the dipole heads in such a way to optimize the tracking of the ion beam along its path (§6).

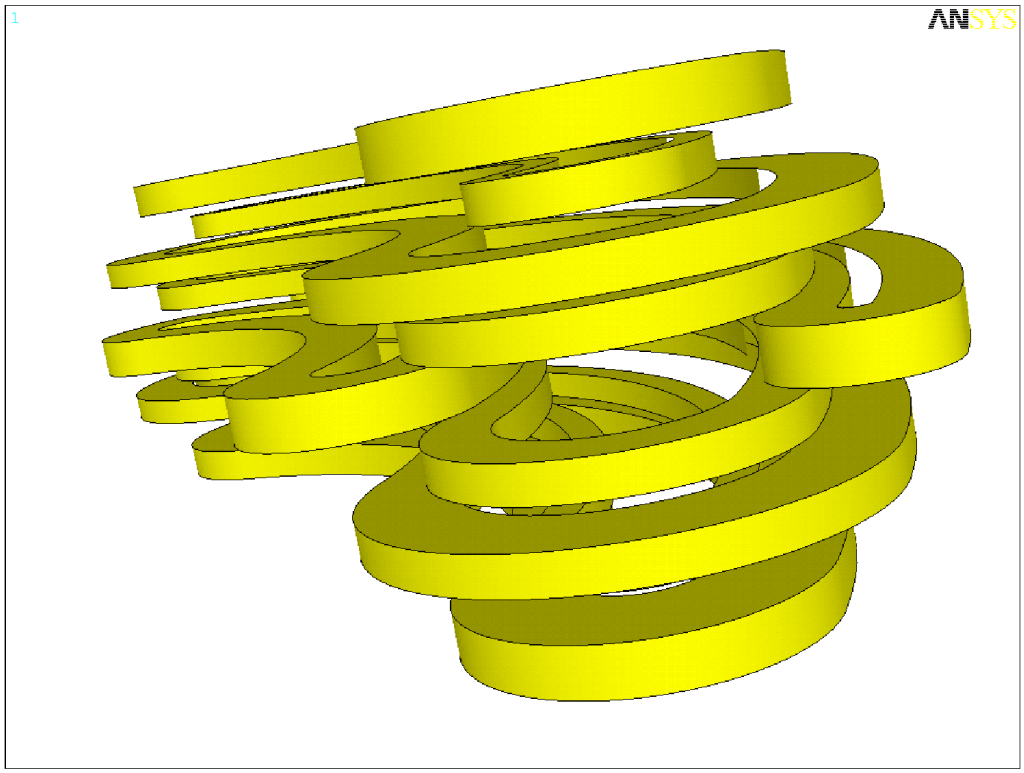

FIG. 6: Perspective 3D view of the superconducting dipole.

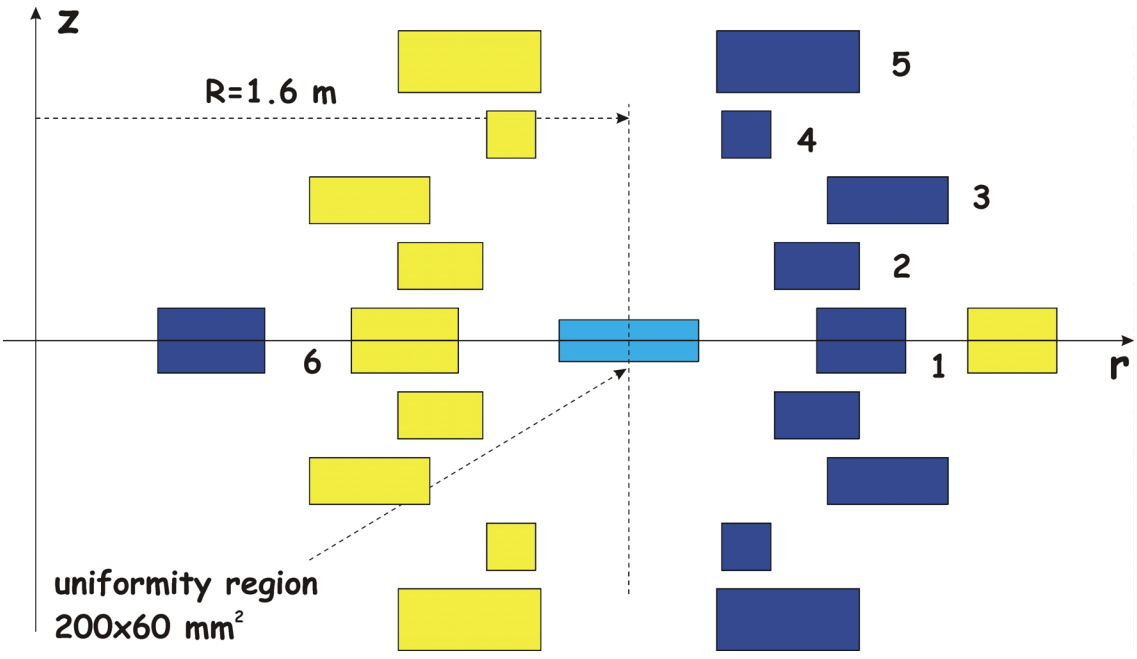

FIG. 7: Section of the dipole far from the ends.

5.1 Design constraints

In the following paragraphs the design constraints identified by the preliminary analysis are listed, with a brief explanation of their meaning and consequences. Moreover, it will be accounted for how we included them in the final optimization.

5.1.1 Central field

The nominal central field should be kept as near as possible to 4 T. This is the less stringent constraint, since, within a limited range, it can be varied by modulating the input current.

5.1.2 Operative current

Due to the poor available refrigerating power, the maximum operative current should be kept within 1000 A, as it will be better explained in §9.

5.1.3 Peak field in the winding

As it is known, the superconducting state strictly depends on three parameters: temperature, current and magnetic field. As function of temperature and magnetic field, it is possible to identify a critical current surface $I_C(B,T)$ that distinguishes between the superconducting state and the normal state. Since the temperature dependence of that surface is nearly linear, as shown in fig. 8, it follows that:

$$I_C(B,T) = I_C(B)\frac{T_C - T}{T_C - T_0}, \qquad (1)$$

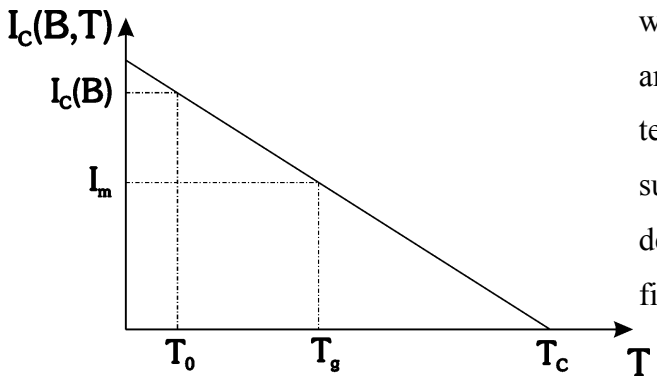

FIG. 8: Critical current $I_C(B,T)$ as function of temperature.

where T_0 is the operating temperature and T_C is the critical temperature, i.e. the temperature above which the superconducting state is completely destroyed independently on magnetic field and current. It is defined as:

$$T_C = T_{C0}\left(1 - \frac{B}{B_{C2}}\right)^{0.59}, \qquad (2)$$

where T_{C0}=9.25 K, and B_{C2}=13.9 T.

If I_m is the operating current, it is possible to define T_g, the sharing temperature, i.e. the temperature at which the superconductor starts to dissipate. It can be easily found that:

$$T_g = T_C - \frac{I_m}{I_C(B)}(T_C - T_0). \quad (3)$$

The difference between the sharing temperature and the operating temperature represents the temperature margin, which is the temperature increase needed to have power dissipation in the coil. Clearly the temperature margin depends on the maximum field experienced by the superconductor: the higher will be that field, the lower will be the temperature margin. In our case, to ensure a safety temperature margin greater than 1 K, the peak field should be around 5.5 T; in fact, introducing in eqs. (2) and (3) the values T_0=4.5 K, I_m=1000 A, B=5.5 T, I_C(4.5 K, 5.5 T)=2712 A, it follows that T_C=6.87 K and T_g=6.00 K, i.e. a temperature margin of 1.5 K. The natural consequence is a new constraint on the model, $B_{peak} \leq 5.5$ T.

5.1.4 Operative current density

Another requirement is on the operating current density, defined as the operating current divided by the conductor cross section. Theoretically, that current density could be

TAB. II: Characteristics of existing magnets.

magnet	location (year)	central field (T)	current (A)	conductor dimensions (mm^2)	current density (10^8 A/m^2)
CDF	FNL (1984)	1.5	5000	3.9×20	0.64
TOPAZ	KEK (1984)	1.2	3650	3.6×18	0.56
ZEUS	DESY (1988)	1.8	5000	4.3×15	0.78
ALEPH	CERN (1986)	1.5	5000	36×3.5	0.40
DELPHI	CERN (1987)	1.2	5000	4.5×24	0.46
BABAR	SLAC (1995)	1.5	5000	4.9×20	0.51
ATLAS	CERN (2005?)	4.0	20000	70×7	0.41
CMS	CERN (2005?)	4.0	20000	30×22	0.30
GANTRY		**4.0**	**1000**		**0.6/0.7**

very high, up to $10^8 \div 10^9$ A/m^2, but it emerges clearly from Tab. II that the existing or under construction magnets all have current densities of the same order of magnitude, $(0.3 \div 0.8) \cdot 10^8$ A/m^2. To be conservative, we decided to choose a current density at the higher limit of that range, but anyway inside it: $(0.6 \div 0.7) \cdot 10^8$ A/m^2.

5.1.5 Conductor

Having fixed the operating current, I=1000 A, and the current density $J=(0.6 \div 0.7) \cdot 10^8$ A/m^2, the same in all the coils, it comes immediately the conductor cross section: $A = \frac{I}{J} = (14 \div 17)\ \text{mm}^2$. Choosing an appropriate aspect ratio for the conductor itself, about 1.5, we finally defined the conductor cross section as 5×3 mm^2.

The conductor to be used to wind the bending dipole is then shown in Fig. 9. It is composed of a Rutherford cable obtained by cabling 6 multi-filamentary NbTi/Cu wires 0.8 mm in diameter. The Rutherford is then embedded in a pure aluminum stabilizer through a co-extrusion or conform process. The characteristics of the conductor are shown in Table III.

TAB. III: Conductor characteristics.

Conductor overall dimensions (non insulated)	3.0×5.0 mm^2
Stabilizer	pure Al
Strand diameter	0.8 mm
Filament diameter	< 10 μm
Cable dimensions	1.6×2.4 mm^2
Number of strands	6
Strand twist pitch	2 cm
Cable twist pitch	5 cm
Cu/Sc ratio	1.5
Critical current at 4.2 K and 5 T	3400 A
Critical current at 4.5 K and 5.5 T	2712 A
Sharing temperatures at 1000 A	6.00 K
Sharing temperatures at 750 A	6.92 K

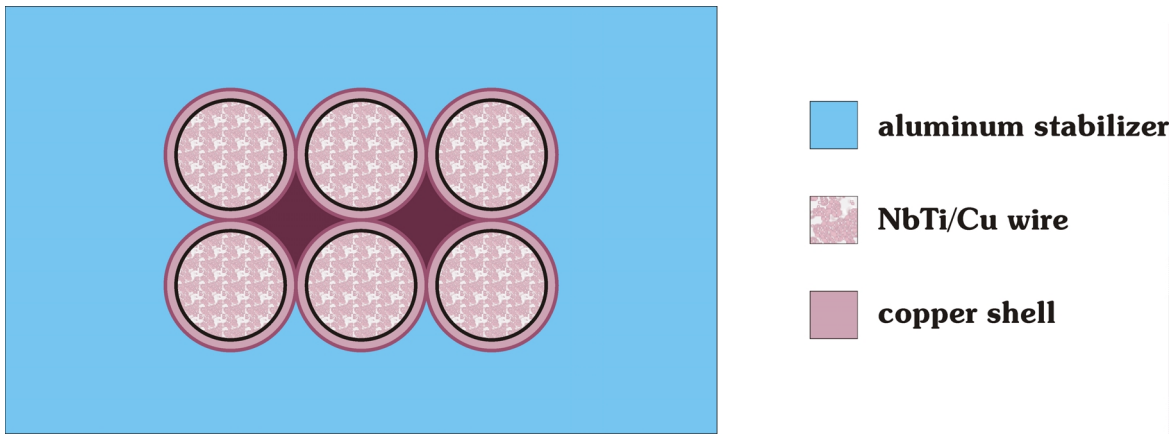

FIG. 9: Layout of the conductor to be used in the winding.

5.1.6 Total inductance

The limitation on the total magnet inductance is due to the fact that we should keep as low as possible the induced voltage during magnetic field variations and the hot spot temperature, as it will be better explained in the following two paragraphs. We found that a reasonable higher limit for the total inductance is 25 H.

5.1.6.1 Induced voltage

Supposing that the scanning in depth could be obtained by varying the beam energy, it follows that, to maintain the correct beam curvature radius, the magnetic field should be varied as well. Considering a magnetic field variation of 0.025 T/s, and then a current ramp of $0.025 \cdot \frac{1000}{4} = 6.25\ \text{A/s}$, the induced voltage is given by:

$$V_{ind} = L\frac{dI}{dt} = 25\ \text{H} \times 6.25\ \text{A/s} = 156\ \text{V}\,. \qquad (4)$$

That value is quite high, for a typical superconducting magnet, and implies the need of a fairly large power supply. The possibility to allow an inductance value larger than 25 H cannot be taken under consideration.

5.1.6.2 Hot spot

The hot spot temperature i.e. the maximum temperature reached by the propagating normal zone, is strictly related to the protection technique. Let us consider the protection scheme shown in fig. 10. The magnet is represented by inductance L; the dump resistor, connected across the magnet terminals, is represented by R. The switch is opened when a non-recovering normal zone, represented by r, appears within the magnet. The stored magnetic energy at the magnet operating current I, given by $LI^2/2$, is then discharged through the dump resistor. It is possible to demonstrate that the maximum hot spot temperature T_{max} is given by:

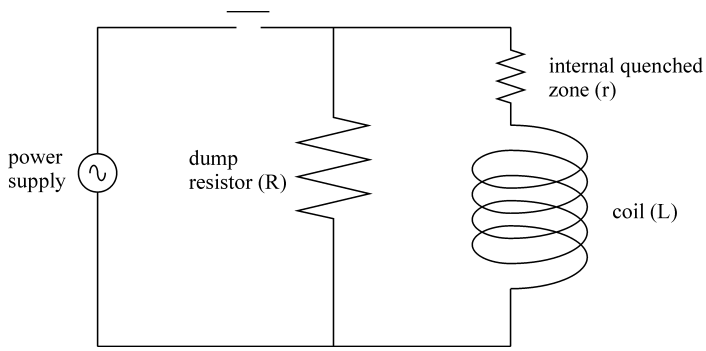

FIG. 10: Magnet circuit for the detect-and-dump active protection.

$$J^2 \frac{L}{2R} = \int_{T_0}^{T_{max}} \frac{C(T)}{\rho(T)}, \qquad (5)$$

where J is the current density, T_0 the operating temperature, C(T) the conductor heat capacity and ρ(T) the matrix metal resistivity.

Introducing in eq. (5) the proper parameters ($J=0.6\cdot10^8$ A/m^2, L=25 H, T_0=4.5 K) and supposing a dump resistor of 1 Ω, the result is that the maximum temperature of the hot spot is T_{max}=233 K and the average temperature is T_{ave}=80 K. Since the maximum temperature is less than the room temperature, and the average temperature is about the liquid nitrogen temperature, that result can be considered excellent.

5.1.7 Overall dimensions

The overall dimensions of the bending dipole make up a further constraint. In fact one of the main reasons to choice a superconducting dipole is the possibility to reduce considerably the overall dimension of the rotating gantry. Secondarily, the radiation losses depend linearly on the external surface and the conduction losses depend linearly on the mass, and then on the volume. We decided to keep within 1 m^2 the area of the minimum

rectangle containing in section all the coils composing the dipole.

5.1.8 Aspect ratio of the single coil

Due to the particular technique proposed by Ansaldo Superconduttori to wind the bent racetrack coils, explained in §7, a particular attention should be kept on the racetrack coil aspect ratio L_r/L_z (see fig. 11). In order to reduce possible risks during the winding operations, it was decided to keep the aspect ratio below 2.5÷2.6.

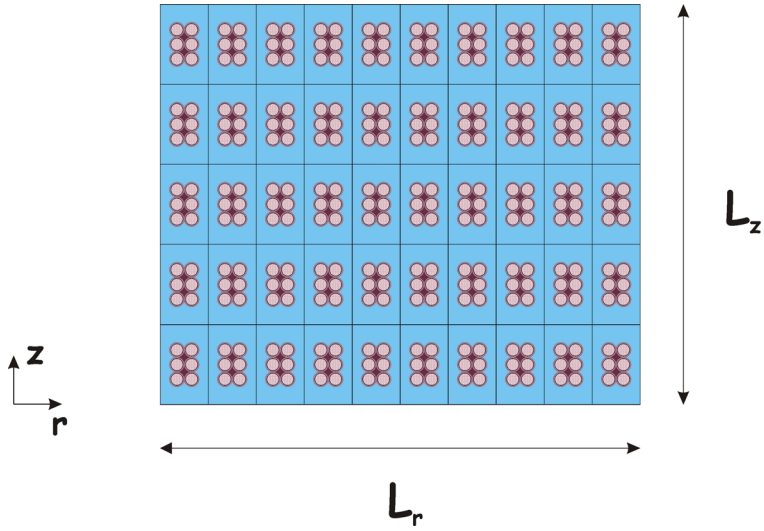

FIG. 11: Aspect ratio of a single coil: L_r/L_z.

5.1.9 Stray field

The stray field is the last constraint we found in this preliminary design, and it has to be taken inside the limits imposed by Italian law for hospital environment. Even if we are aware of the problem, we decided to postpone its solution; actually several possibilities are under study, as compensating coils or a cryostat made by iron, but none of them was implemented in the optimization algorithm.

5.2 2D optimization – the genetic algorithm

The genetic algorithms are adaptative methods that, imitating the evolutionary processes theorized by Darwin, are able to solve very complex optimization problems, and result particularly efficient when handling:

- topologically very complicated surfaces, even non continuous or non derivable and in presence of a large number of local maxima or minima;
- a large number of independent variables, both discrete and continuous.

With respect to the conventional optimization techniques, which usually stop when a local

minimum (or maximum) is found, the genetic algorithms have a much larger probability to converge on an absolute minimum (or maximum).

Those methods are based on the generation of a sequence of populations, constituted by a large number of individuals, i.e. solutions to the specific optimization problem. Every individual is valuated on the basis of its fitness, i.e. a parameter that determines the probabilistic selection of the individuals worth to act as "parent" of the next generation.

The genetic evolution of the population is based on the genetic operations *mutation* and *crossover*, which allow recombining the genetic code of individuals, usually encoded in binary notation. The probability that the last produced generations are constituted by individuals whose fitness is nearly maximum rises with the increasing of the reproduction number. When the reproducing cycle is finished, the result is not one only optimal solution, but a complete population of quasi-optimal solutions, often very different one to each other.

Since our problem contains a large number of design variable (both continuous and discrete) and very complex constraints (on dependent and independent variables), the choice of the optimization method converged very soon on a genetic algorithm. Then the Finite Element code ANSYS[13)] was linked to the algorithm: for every individual, ANSYS performs a magneto-static analysis, calculating the field uniformity in the rectangular region 200×60 mm^2 and assigning a fitness value to the considered individual. Then the process control returns to the genetic algorithm.

5.3 2D Finite Element model

The axis-symmetric finite element model used to perform magneto-static analyses is shown in fig. 12. The lower boundary of the model, corresponding to the dipole equatorial plane, is a symmetry plane; the left boundary of the model coincides with the cylindrical symmetry axis. That model is made by 20˙000 PLANE53 elements and 200 INFIN110; it needs 20 seconds CPU time for a single run on a Workstation COMPAQ XP100, and about 12 hours CPU time to obtain 100 generations of the considered population (2˙000 individuals). The INFIN110 elements allow modeling an "open boundary": a single layer of those elements simulates the whole semi-infinite domain that surrounds the region actually meshed by PLANE53 elements.

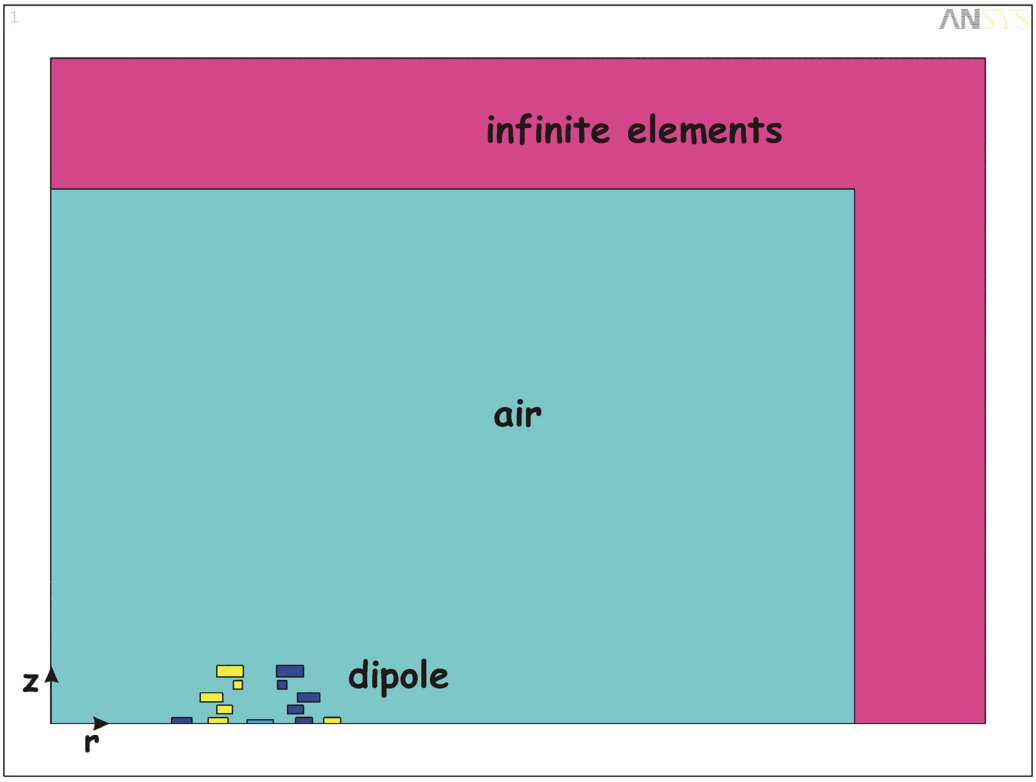

FIG. 12: The axis-symmetric finite element model.

The parameters taken up as design independent variables are:

- the number of turns in the z direction for every coil (5 variables, assuming the same value for the two coils on the equatorial plane);
- the aspect ratio of every coil (6 variables);
- the aperture, i.e. the radial distance between the two circular arcs of every coil (6 variables);
- the distance between the two circular arcs of the equatorial coils (2 variables);
- the axial distance between two adjacent coils, supposed to be equal between all the coils (1 variable).

The total number of independent variables is 20.

It is important now to explain how we took into consideration the eight constraints arisen during the preliminary analysis. Two of them, the aspect ratio and the overall magnet dimensions, are simply verified by imposing opportune limits on the corresponding design variables. Imposing their right values solves the constraints regarding independent design variables: then the coil sections will be multiples of the conductor section (5.2×3.2 mm^2

insulated), the current will be 1000 A, and the current density $J = \frac{1000\ \mathrm{A}}{5.2 \times 3.2\ \mathrm{mm}^2}$ $= 0.6 \cdot 10^8\ \mathrm{A/m}^2$.

The last three design requirements (central field, peak field on the winding and inductance) are derived parameters and then cannot be imposed a priori. They depend on the Finite Element result and the genetic algorithm controls them by introducing opportune penalty functions. The choice of the penalty functions was very complicated and required lots of refinements. The final formulation of the function O to be minimized is:

$$O=U+P_1+P_2+P_3, \tag{6}$$

where U represents the field uniformity and P_1, P_2 and P_3 are the penalty functions, defined as:

$$\begin{cases} P_1 = \left[(4 - B_0)/B_0\right]/f_1 & \text{applied if } B_0 < 4\ \mathrm{T} \\ P_2 = \left[(B_{peak} - 5.5)/5.5\right]/f_2 & \text{applied if } B_{peak} > 5.5\ \mathrm{T} \\ P_3 = \left[(L - 25)/25\right]/f_3 & \text{applied if } L > 25\ \mathrm{H}. \end{cases} \tag{7}$$

$f_1=10$, $f_2=f_3=100$ are three factors that reduce the penalty and are chosen on the base of the severity of the corresponding constraint.

5.4 Final results

The optimization procedure driven by the genetic algorithm produced more than 20 solutions, distinguished by substantial geometric differences and providing acceptable values of field uniformity (less than 2‰), fulfilling all the design requirements. Among them, the best one has a uniformity of 0.85‰, with B_{peak}=5.1 T, and L=24.5 H. The central field is 4.000 T, by imposing a current I=993 A. In fig. 13 and 14 the flux lines and the magnetic field area respectively shown.

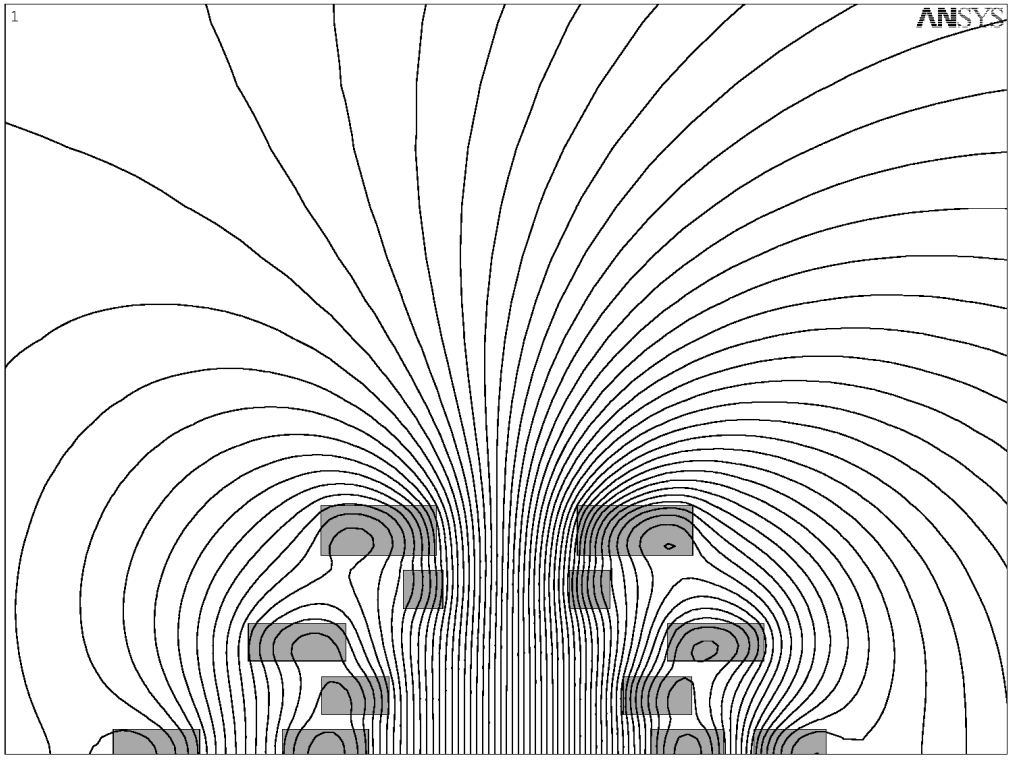

FIG. 13: Flux lines of the best configuration (0.85‰ in uniformity).

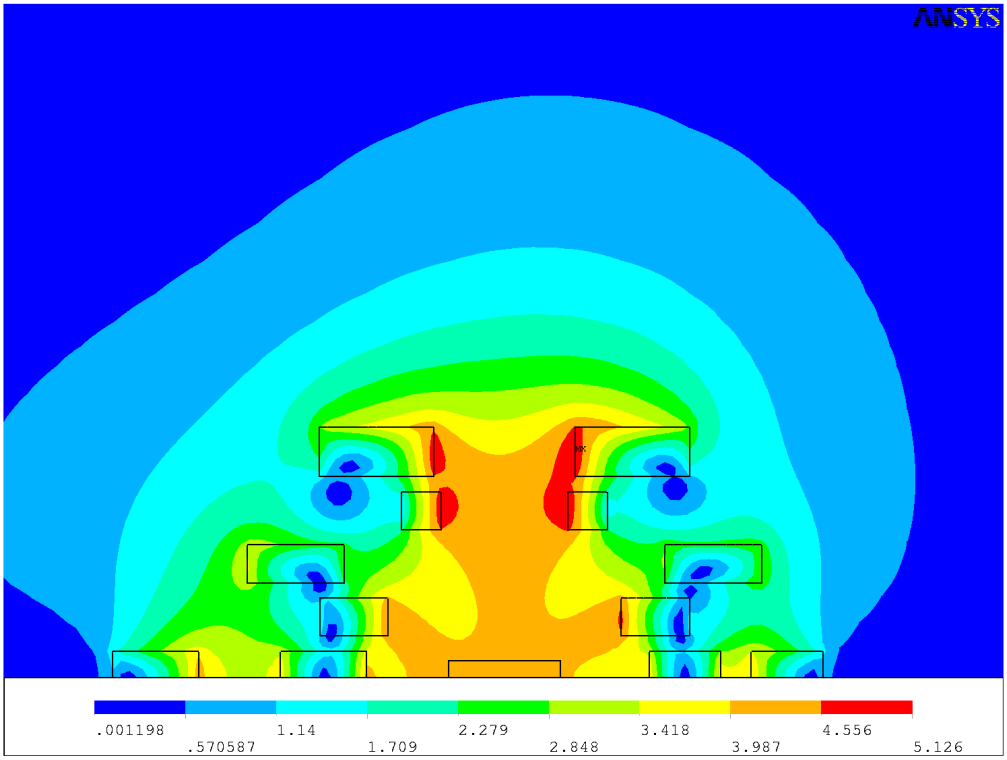

FIG. 14: Magnetic field map of the best configuration (0.85‰ in uniformity).

6. 3D LAYOUT

Passing to the 3D model, our attention was focused on the beam tracking. In this frame it is important to have at the patient location the same beam geometry entering into the dipole. The most of the work was then devoted to the optimization of the dipole heads. The 3D model was developed by using the Finite Element code OPERA 3D[14] (fig. 15).

In fig. 16 a typical beam spatial distribution is given.

As first step, we studied the effect of the heads on the magnetic field uniformity and verified the tracking of a beam of carbon ions. We used as variable the trajectory, which represents the ideal path of a carbon ion inside the dipole, exactly at the center of the good field region of 200×60 mm^2 (see fig. 17).

The 200×60 mm^2 regions are quadrilateral patches perpendicular to the beam trajectory, which intersects the patches exactly at their center. In fig. 18 we can see both the magnetic field intensity perpendicular to the beam trajectory (B_x) along this line and the field uniformity in the same position.

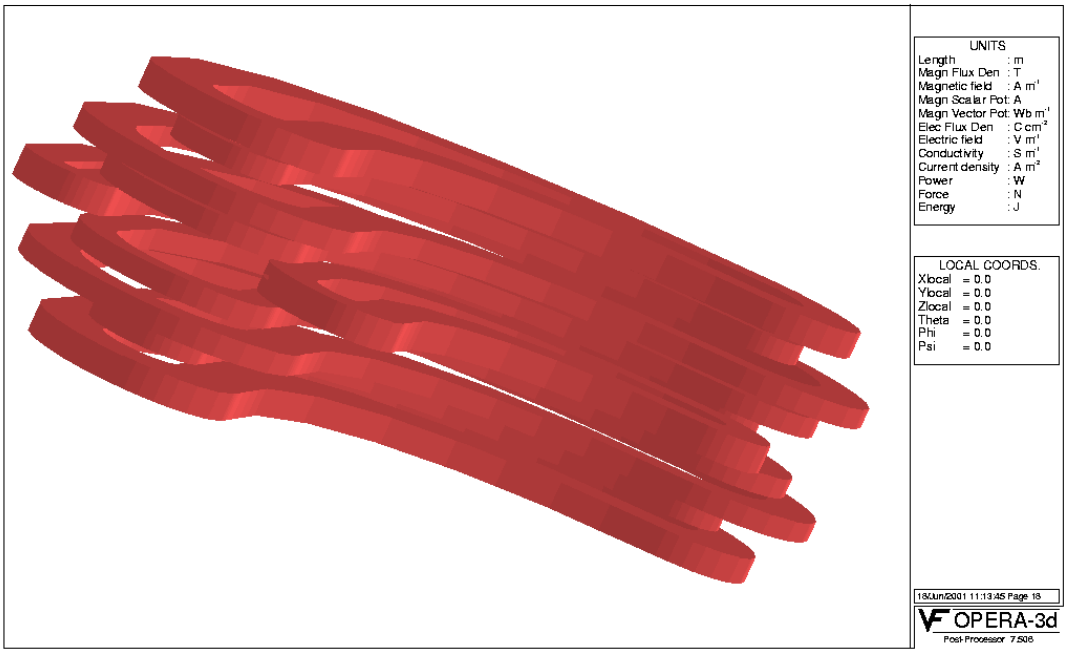

FIG. 15: 3D distribution of the coils.

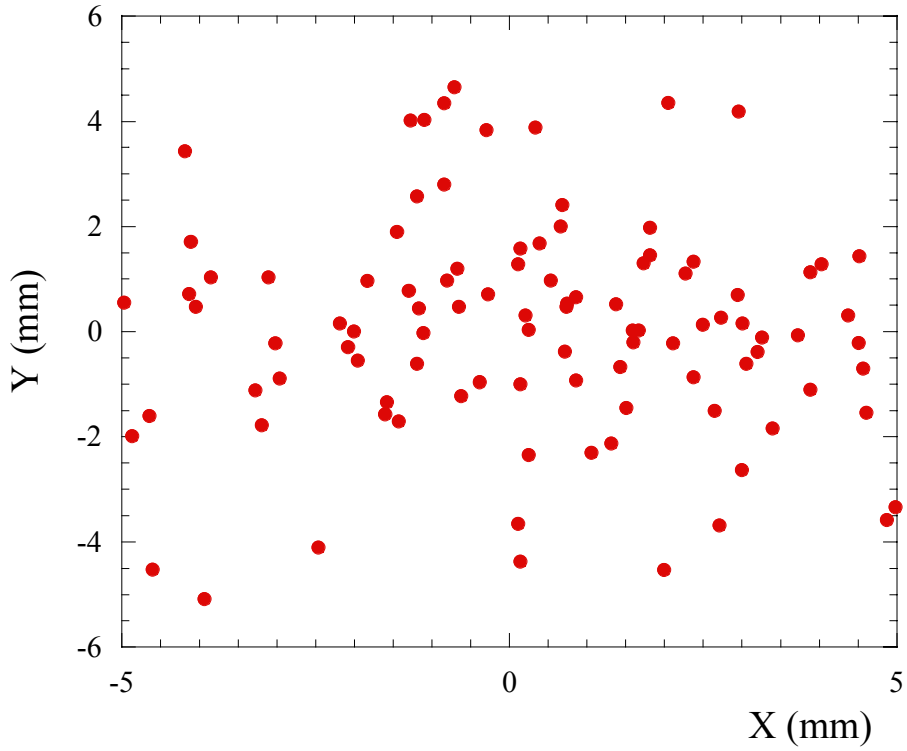

FIG. 16: Typical spatial distribution of the ion beam, as extracted from the synchrotron.

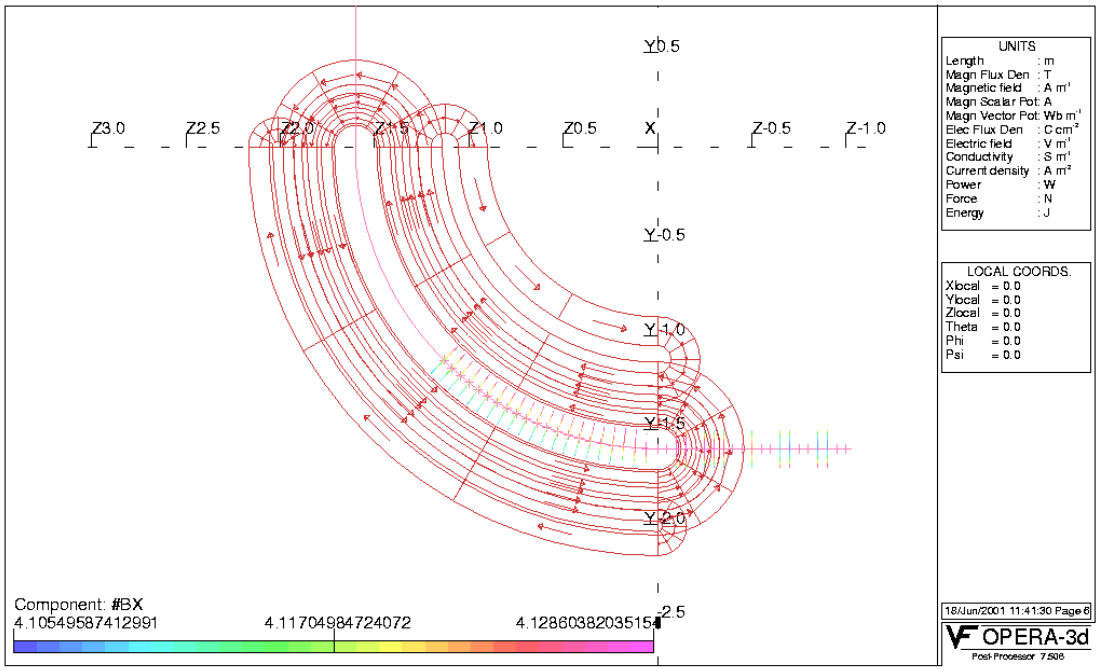

FIG. 17: Trajectory of the ideal ion and position where the field uniformity will be calculated.

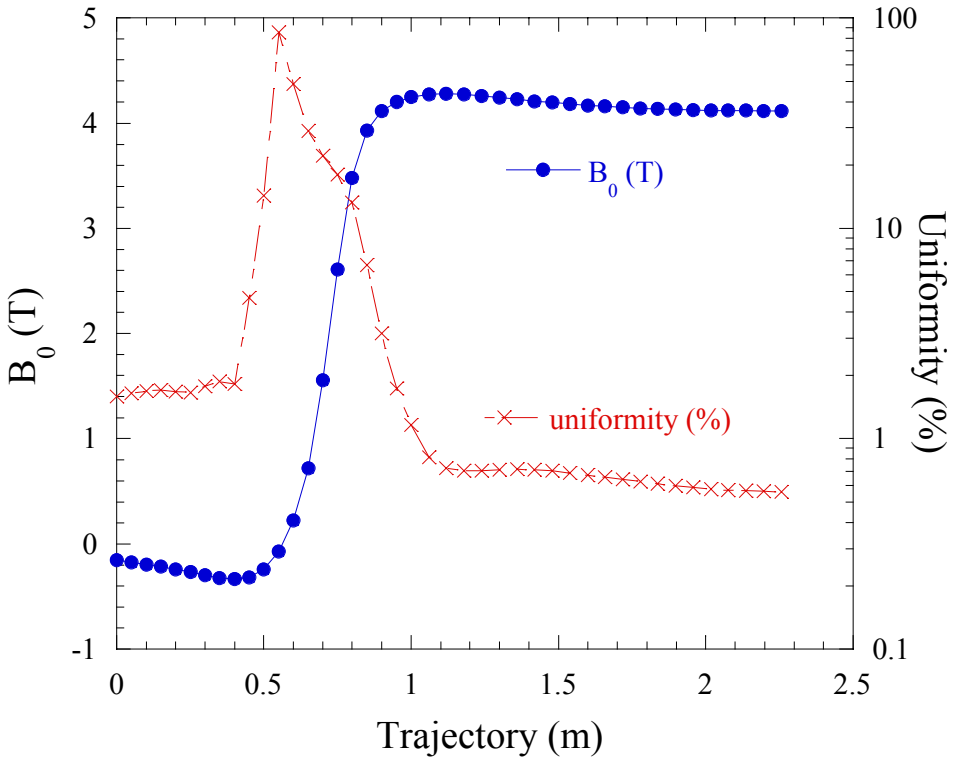

FIG. 18: Central field and field uniformity of the 3D model.

It is clear that the heads influence is not negligible at all. At the center of the dipole the uniformity is 5.61‰, well above the value of the 2D model (0.85‰). To be sure that this difference is a consequence of the head magnetic field, we built a 3D model representing exactly the 2D geometry (360° rings instead of 90° dipoles) and we found the same uniformity.

The worst situation occurs at the head region, where the field uniformity is (10÷30) % and the magnetic field is (3÷4) T. Anyway we tried to see if our dipole is able to bend a carbon ion having energy of 400 MeV/u on a radius of 1.6 m. In fig. 19 we see that in order to have 90° of bending angle the total angle of the dipole must be reduced of about Θ=18°.

As a result of this geometrical change, the ion track is still acceptable but we have a beam deformation due to the poor field uniformity (fig. 20).

The beam deformation can be seen considering a reduced beam made of 10 ions representing the same spatial distribution of the total beam.

Although during the dipole crossing the beam ratio and relative position varies a lot, if we compare the starting and final distribution, the beam almost recovers its shape and relative

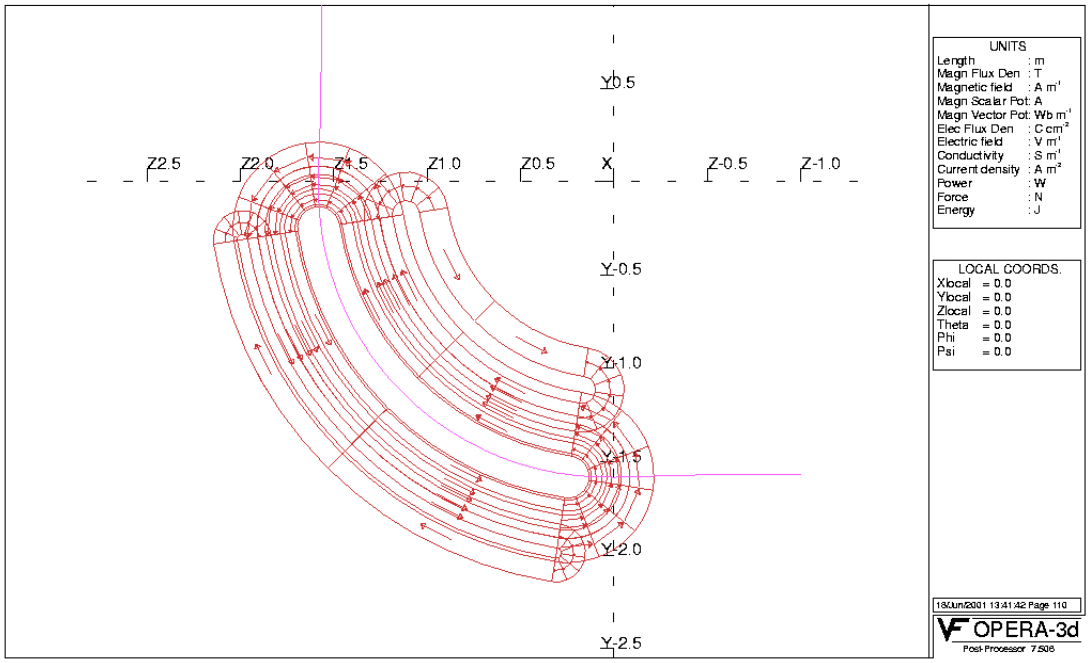

FIG. 19: Tracking of a carbon ion.

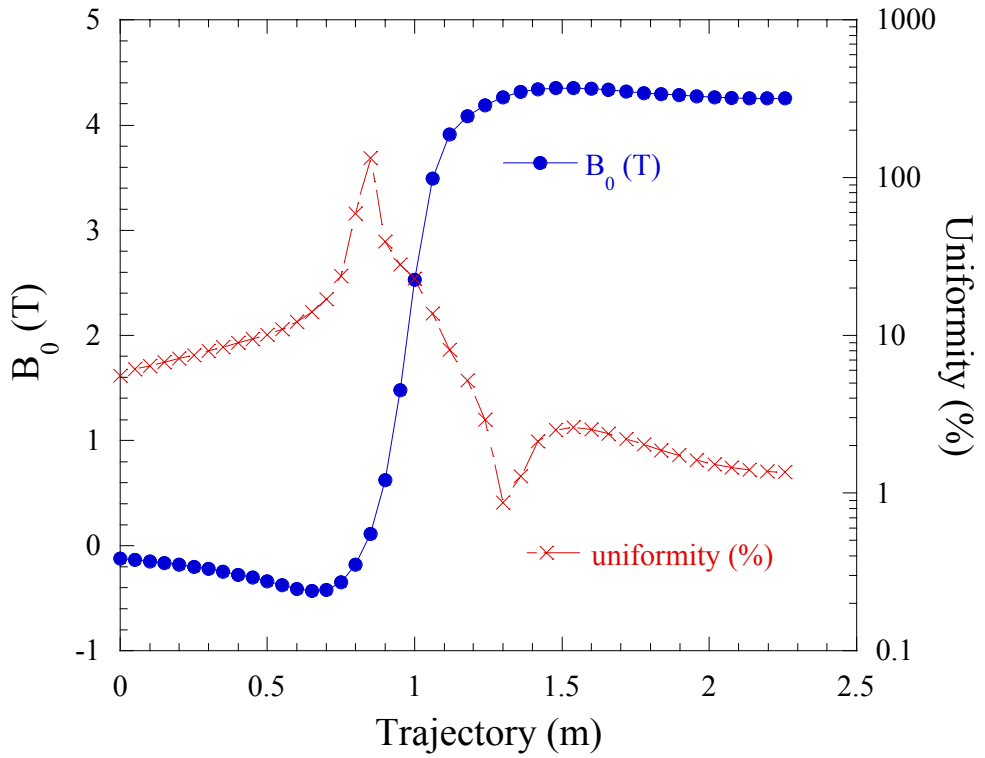

FIG. 20: Central magnetic field and uniformity of the 90-Θ dipole configuration.

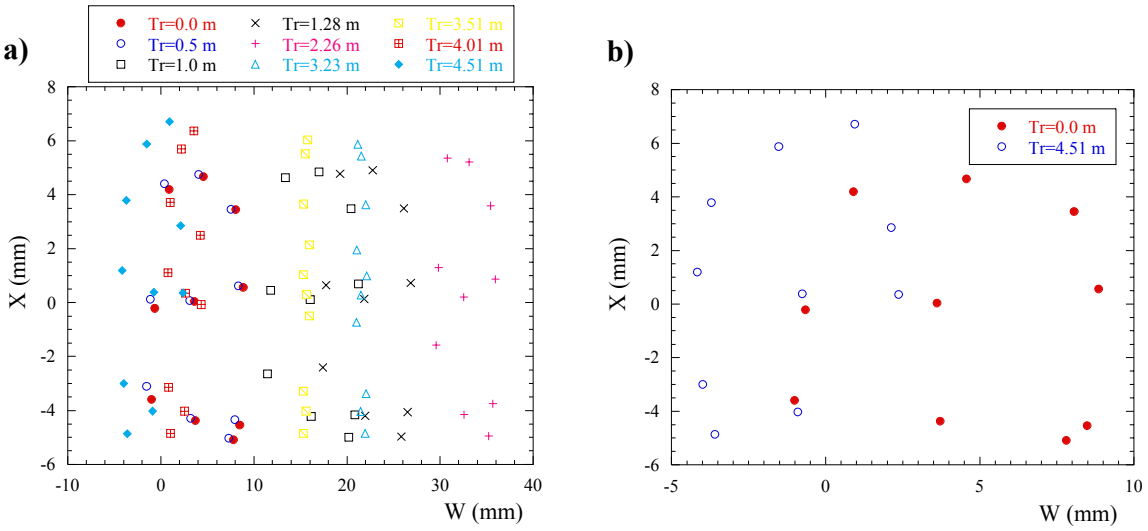

FIG. 21: (a) Beam distribution at different trajectory points. (b) Comparison between the initial point (X=0, Y=-1.6 m, Z=-1.0 m) and the final point (X=0, Y=1.0 m, Z=1.6 m). X is the x-axis of the OPERA coordinate system, W is an axis perpendicular to X and Tr, where Tr is the versor of the curvilinear abscissa. That means that X and W always generate a plane perpendicular to the curvilinear abscissa.

position. Let us now see what happens close to the boundaries of the 200×60 mm^2 region where we plan to move the beam. We have performed this analysis supposing that the focus of the scanning magnet is placed at the position X=0, Y=-1.6 m, Z=-1.0 m.

We used two different scanning angles: Θ_1=3° and Θ_2=-3°. In fig. 22 the results of the beam tracking is showed.

It is evident that there is a problem on the exit of the beams, which are supposed to be parallel. Also the aspect ratio of the beam changes during the track (fig. 23). The initial area of the beam $\Delta X \times \Delta W$ is about 10×10 mm^2. In the case of Θ=0° the area becomes 11.6×6.5 mm^2, for Θ=3° $\Delta X \times \Delta W$=21.5×8.0 mm^2 while for Θ=-3° $\Delta X \times \Delta W$=4.0×4.0 mm^2.

Our actual work is to improve the magnetic field uniformity by using a standard technique in dipole design, a split of the heads. In fig. 24 the model that is in use for each coils is showed. By using the same genetic algorithm described in §5.2 we optimize the field uniformity in the head region, where we have both bad magnetic field uniformity and high values of the magnetic field. The parameters we are optimizing are the distances between the split heads H_i (6 parameters).

Because we are interested in having a good uniformity where the magnetic field is high, but we can accept a bad value of uniformity where the magnetic field is low (less than

0.01 T) we introduce a function $G(B,U)=G_1(B)G_2(U)$ where G_1 is an increasing function of B and G_2 is a decreasing function of U (U is the magnetic field uniformity in %). The goal of the genetic algorithm is to maximize G for different values of the six parameters H_i. Contemporary also the introduction of compensating coils is under study (fig. 25). In this case the geometry of the racetracks and their relative position with respect to the dipole will be studied.

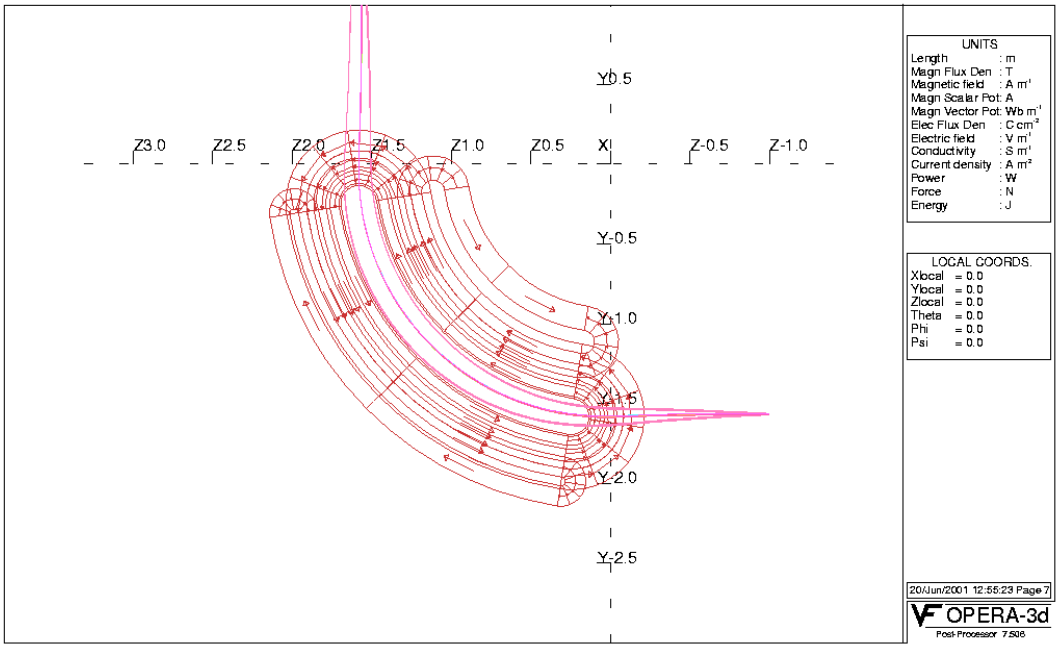

FIG. 22: Beam tracking at three different angles of the scanning magnet, Θ=0, Θ=3°, Θ=-3°.

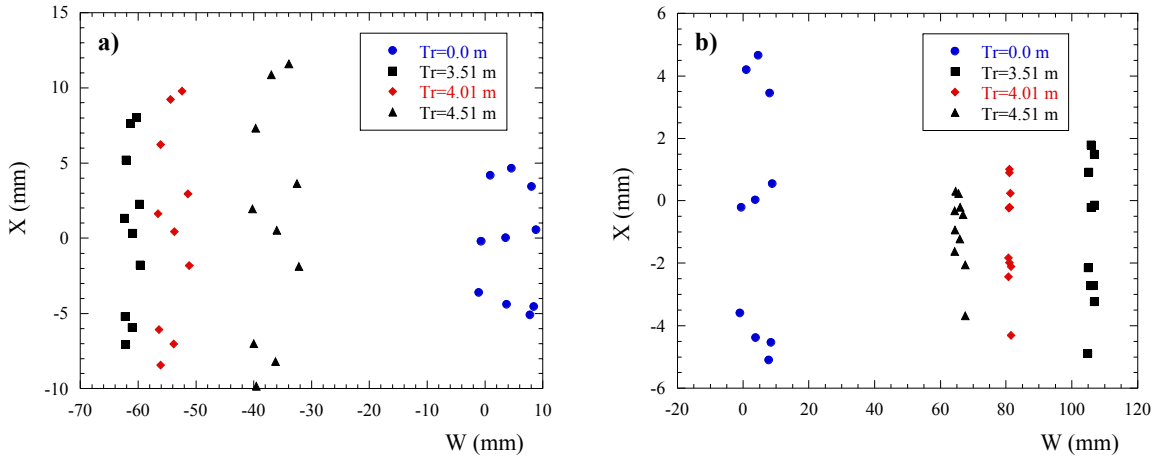

FIG. 23: Beam distribution at several locations along the beam path. a) Θ=3°, b) Θ=-3°.

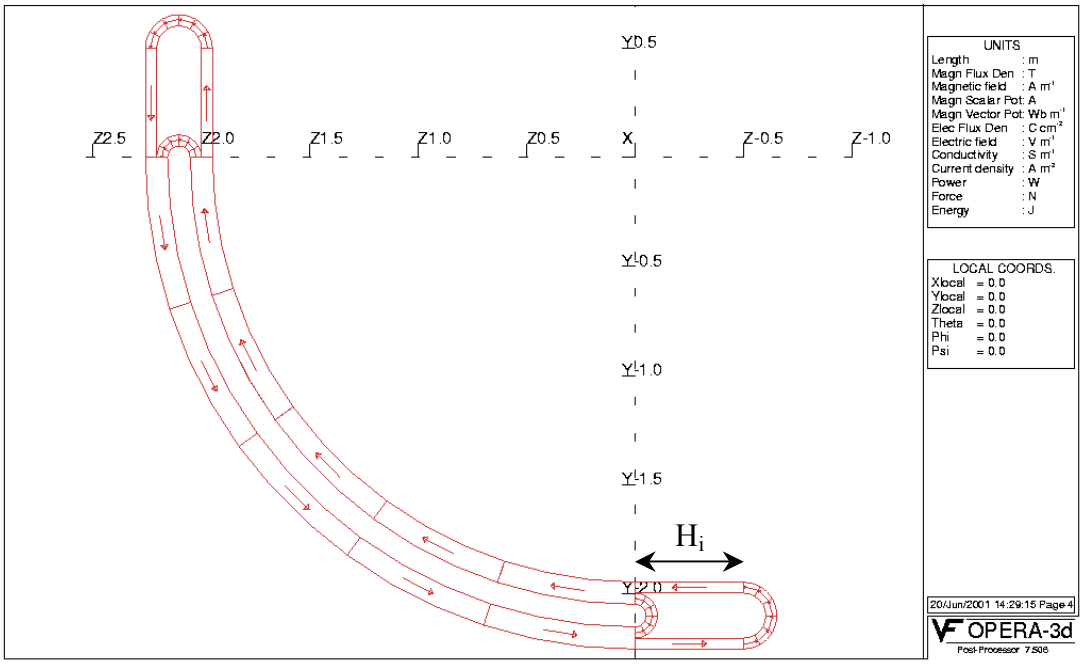

FIG. 24: A coil with split heads.

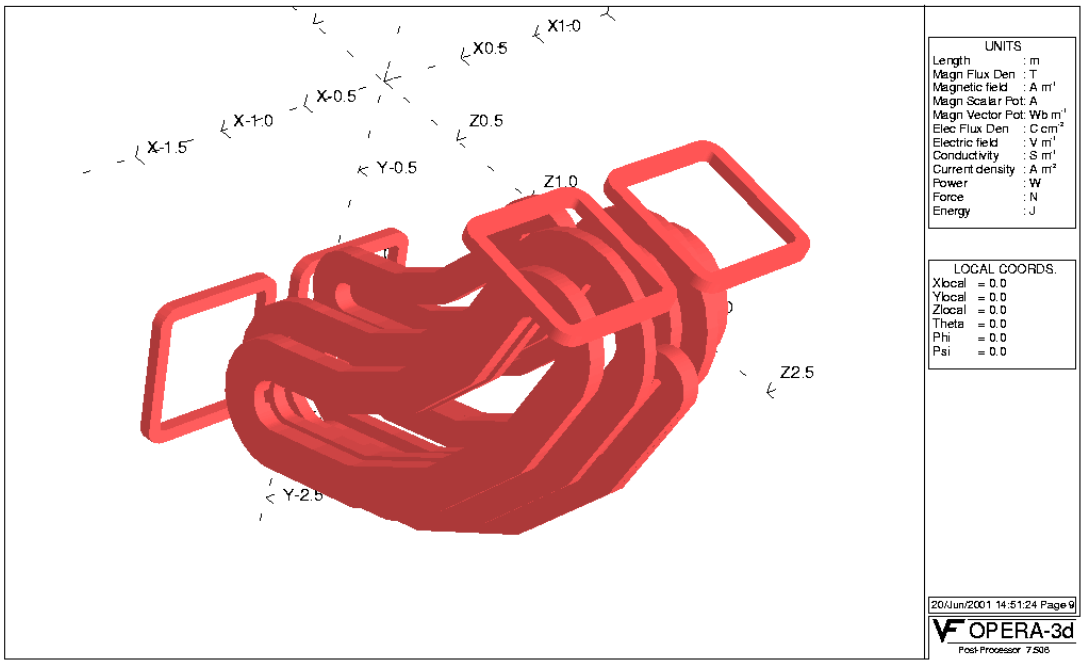

FIG. 25: Dipole model containing the four racetrack compensating coils.

7. WINDING TECHNIQUES

7.1 Generalities

In the frame of the preliminary feasibility study for the TERA/INFN/Gantry magnetic system, Ansaldo Superconduttori is in charge of assessing the manufacturing feasibility of the split coils. Such coils have an aspect that makes them difficult to wind: their shape. In general a racetrack coil, because of its two parallel straight legs, imposes particular care during winding to avoid creating gaps among turns. For the compaction of windings, the racetrack shaped coil cannot take advantage from the hoop stress present in conventional circular solenoids. Here the situation is even worse, because the racetrack coil is curved, and this implies that one of the two legs is concave. Ansaldo Superconduttori already manufactured in the past coil with such shape, but with a much more stiffer and bigger conductor, that allowed an effective temporary keeping in place of wound turns. The gantry coils have instead a rather small conductor, around 5×3 mm^2, that makes turns unable to keep themselves the concave shape. Ansaldo Superconduttori first tried a study of a special tool able to wind this curved dipole, but quickly came to the conclusion that a totally different approach had to be found.

7.2 Proposed winding solution

By analysing the Magnetic System with CAD, a particularity of the Racetrack Curved geometry suggested and made possible an alternative approach for the winding, that appears attractive and much easier from the winding point of view. As shown on fig. 26, the concave profile of the coil, included half of the development of each coil head, is exactly identical to the convex profile of the other leg of the coil, head excluded. This means the concave profile can be replaced with an equivalent convex one, without affecting the overall turn length. As shown on fig. 26, this is true for any profile, and this means that is applicable to all the coil turns. Fig. 26 shows and demonstrates that for two turns, 2163 and 2085 mm long respectively. Moreover, as shown on fig. 27, the constancy of the perimeter is still maintained for coil geometry with the heads split in two sections (to reduce the current density) and the curved legs with two different radii of curvature (100 mm Dr).

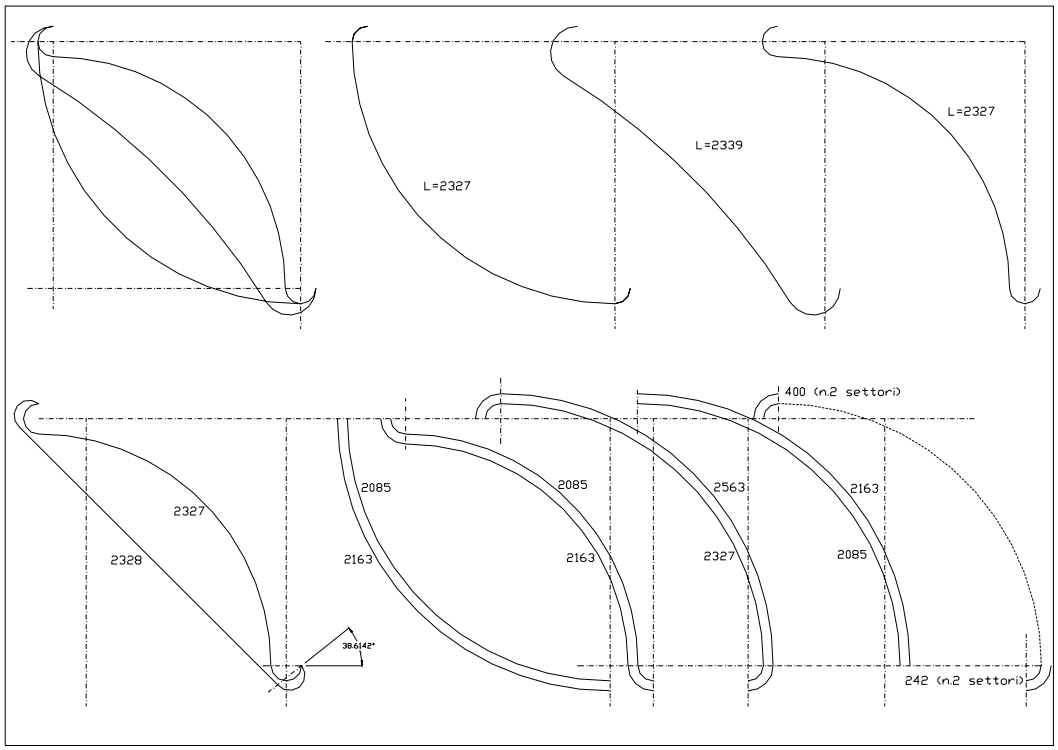

FIG. 26: Test of the equivalence of the profiles.

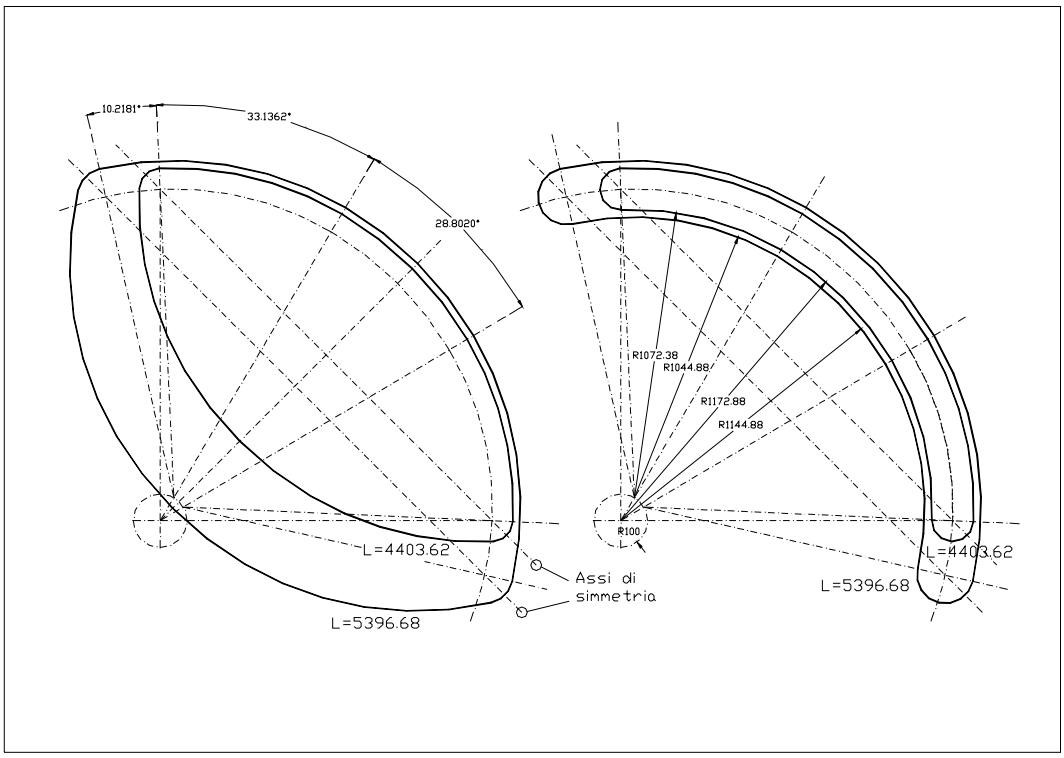

FIG. 27: Test of the equivalence of the profiles for a coil geometry with the heads split in two sections.

This geometric property allows the winding to be made with a simpler and different approach: the coil is wound with the two legs convex and symmetrical, mirrored with respect the coil longitudinal axis. Once all the turns have been wound, the convex leg is pushed and moved gradually toward its final concave profile. This procedure is much more simpler from the mere winding point of view but, as usual, the solving of one problem has to be paid with the rising of another problem, in principle less severe, that is how to safely push the leg in the concave position. This definitely imposes to test all the procedure on a mock-up, to verify the turn matrix is not loosed and damaged during the transferring. As it can be easily understood, during the transferring turns are deformed and consequently submitted to a large mutual slipping. This has to be well controlled in order to avoid creating gaps among turns, that could cause some turns lose irremediably their original design shape.

7.3 Description of the winding method

Basing on the above considerations, the manufacturing sequence, as shown on fig. 28, is the following:

- all turns are wound on a special winding form (described in the next §7.4) that replaces the concave coil leg with its homologue convex shape;
- once the winding is completed, all turns are tighten together by suitable clamps;
- the part of the winding form, relative to the temporary convex leg, is then removed;
- the winding pack is now free to slide on the winding table;
- acting on the clamps, turns are slowly and gradually pushed toward the concave portion on the winding form;
- during this operation turns tend to become loose. To control this effect, the two heads of the winding table are able to rotate and compensate that effect, by keeping winding in tension;
- in order to allow slipping among turns, the compaction given by the clamps is suitably graded and adjusted. Eventually the use of a slipping powder will be considered;
- the 7 clamps used to guide the winding arm during its transition are not disengaged, they reach their final design position and lock and maintain the coil shape.

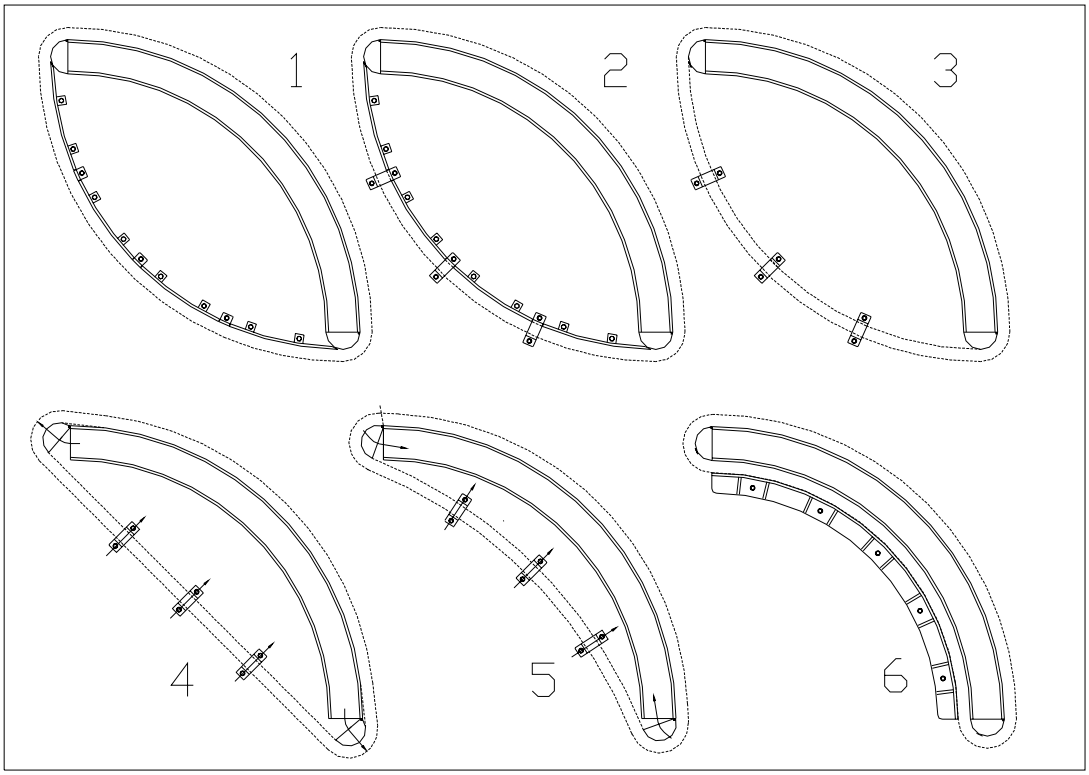

FIG. 28: Winding sequence.

7.4 Description of the winding tool

Figs. 29, 30, 31, 32, 33, 34 and 35 show the layout of the winding tool needed to perform a feasibility test on the above winding method, as well as the various steps of the operation. In particular, fig. 29 shows the tool main concepts and components. The tool is composed of:

1. a winding platform;
2. a steel profile that reproduces the final coil shape, bolted to the winding table;
3. two rotating heads, to compensate the turn loosing during the transition from the convex to concave shape;
4. 8 steel blocks, bolted to the winding table, that create part of the temporary convex profile of the coil;
5. other 7 blocks, that complete the temporary convex profile, but are also arranged to engage with 7 clamps, used for compacting turns during the transferring;
6. 7 plates, bolted to the coil final profile, with the aim to provide, together with the winding table, the side containment for the windings.

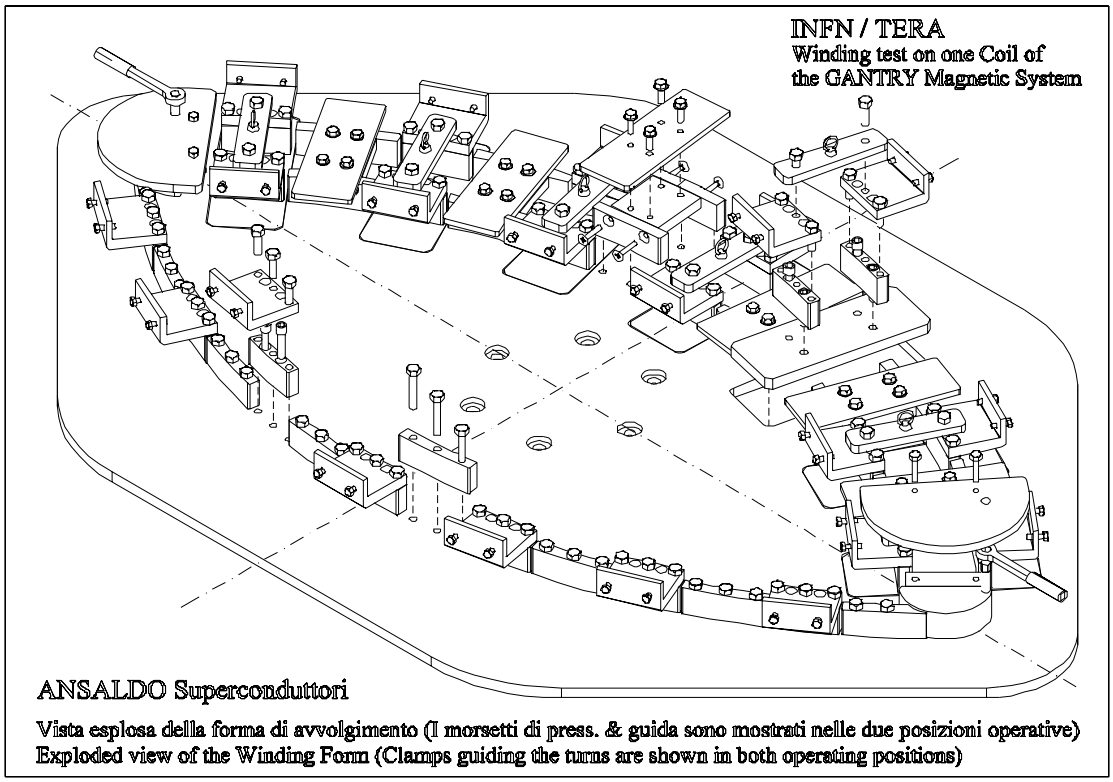

FIG. 29: Exploded view of the winding form.

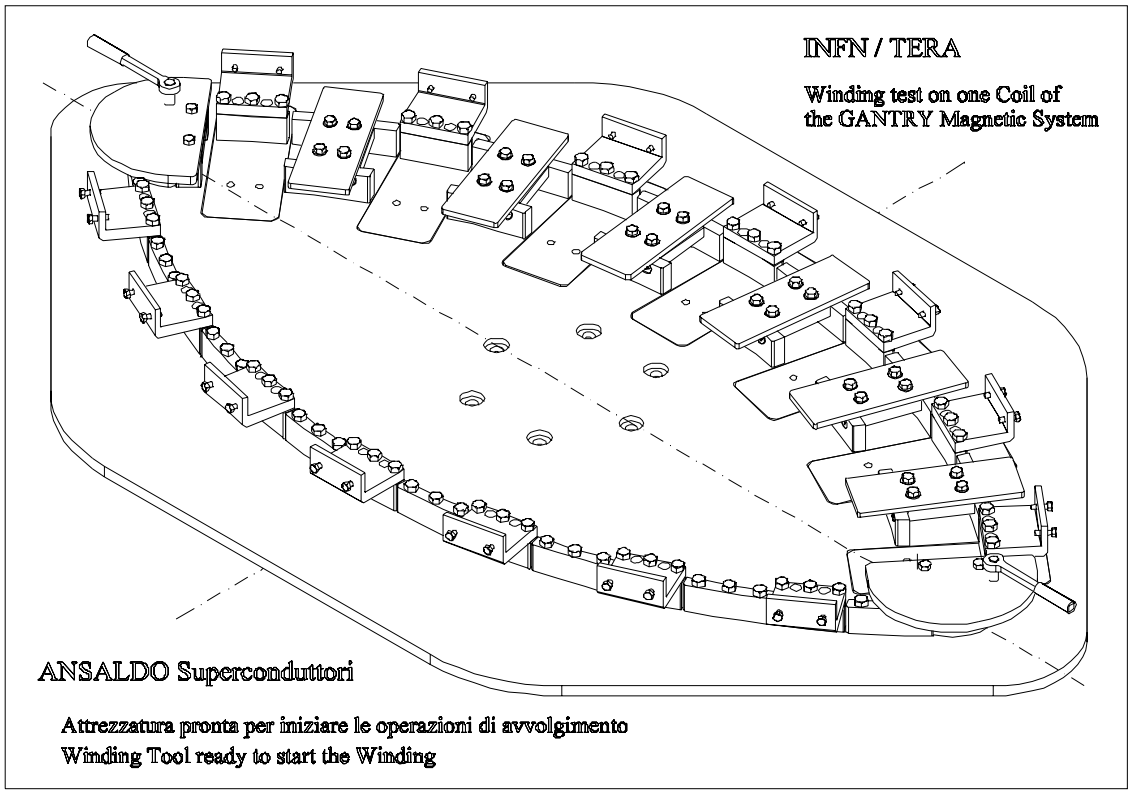

FIG. 30: Winding tool ready to start the winding.

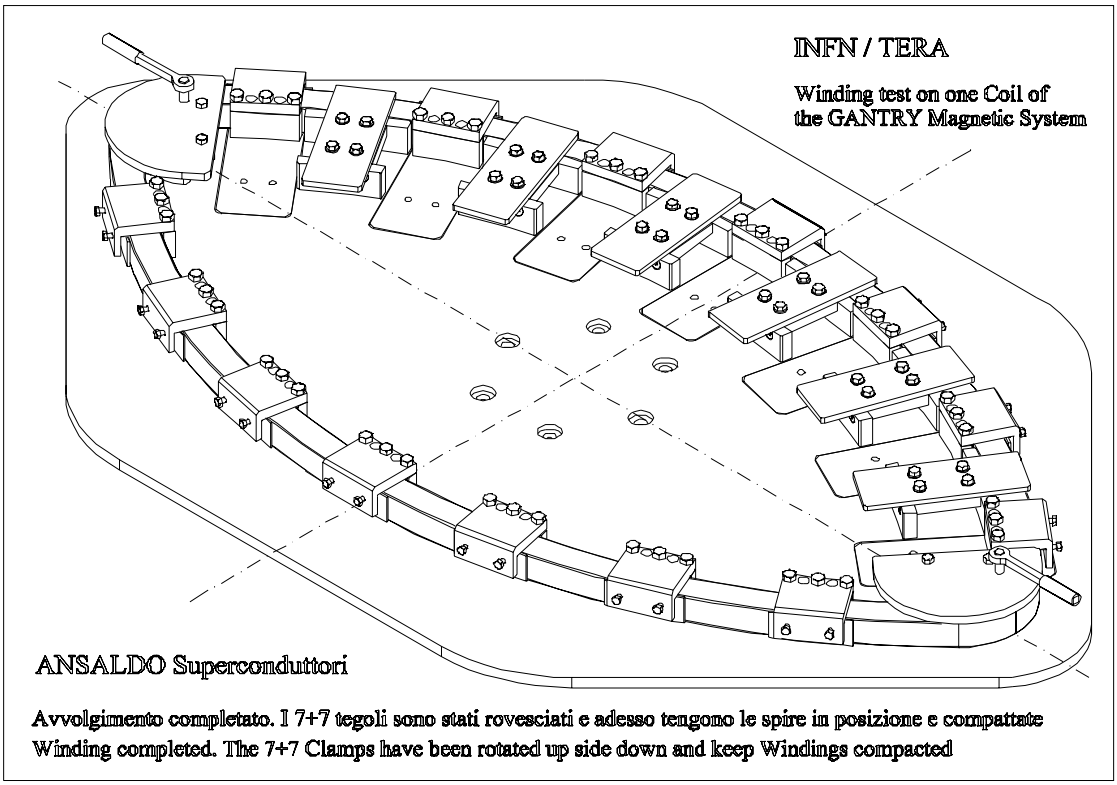

FIG. 31: View of the winding when completed.

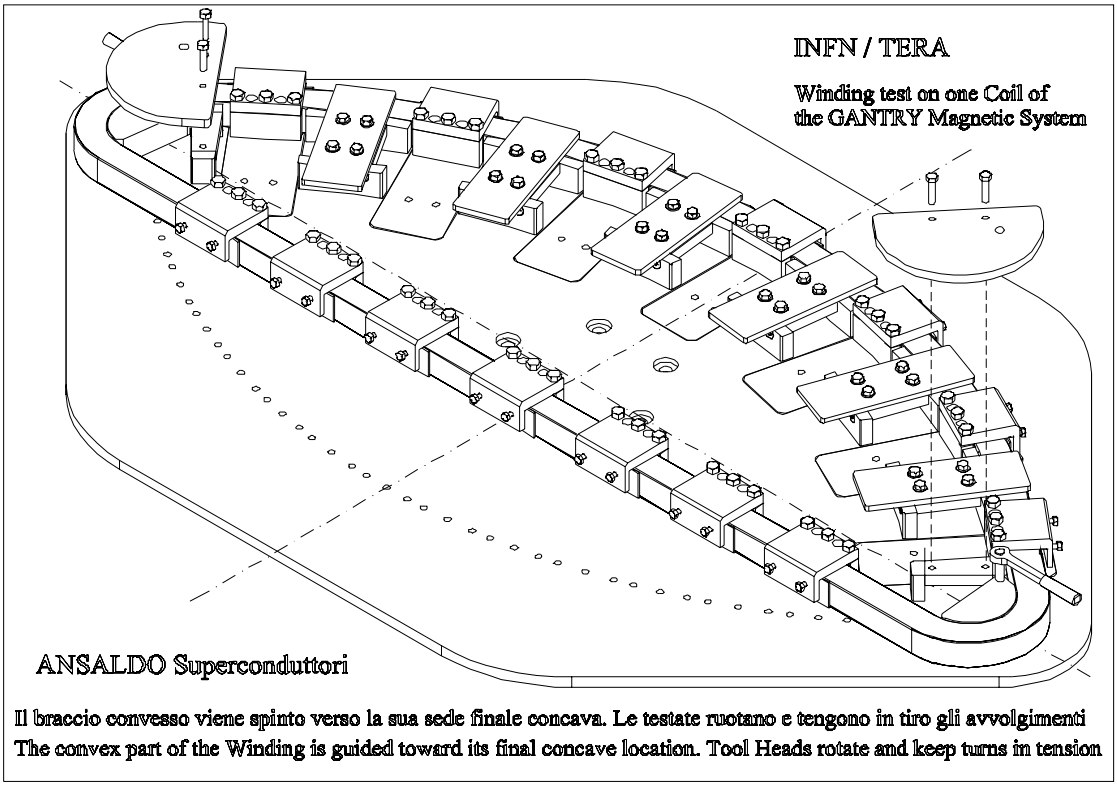

FIG. 32: Coil clamped and free to move toward the winding form concave section.

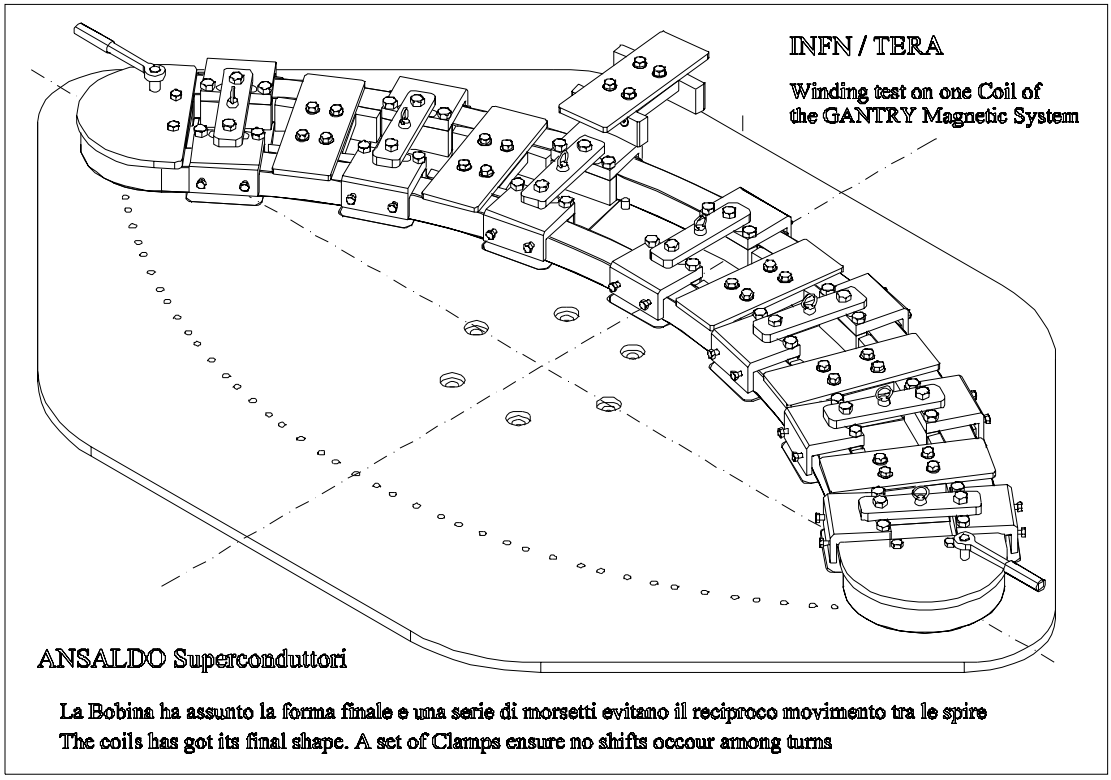

FIG. 33: The coil in its final shape.

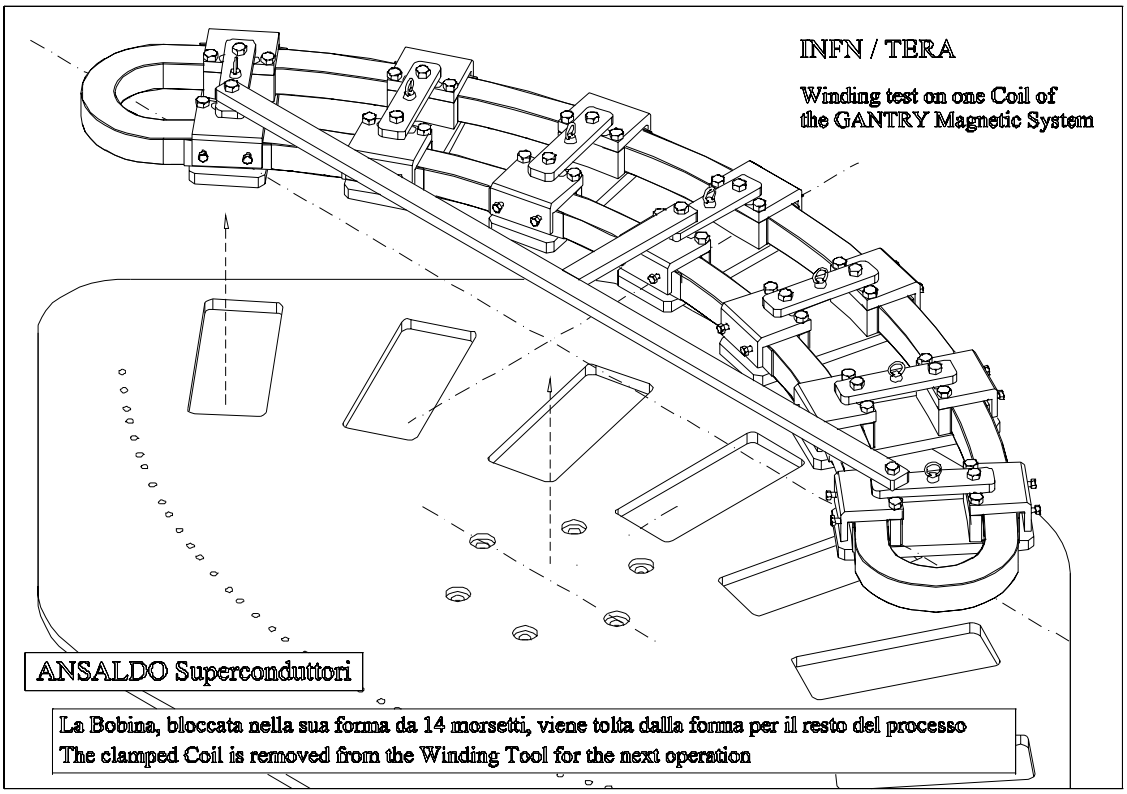

FIG. 34: Clamped coil removed from the winding tool for the next operation.

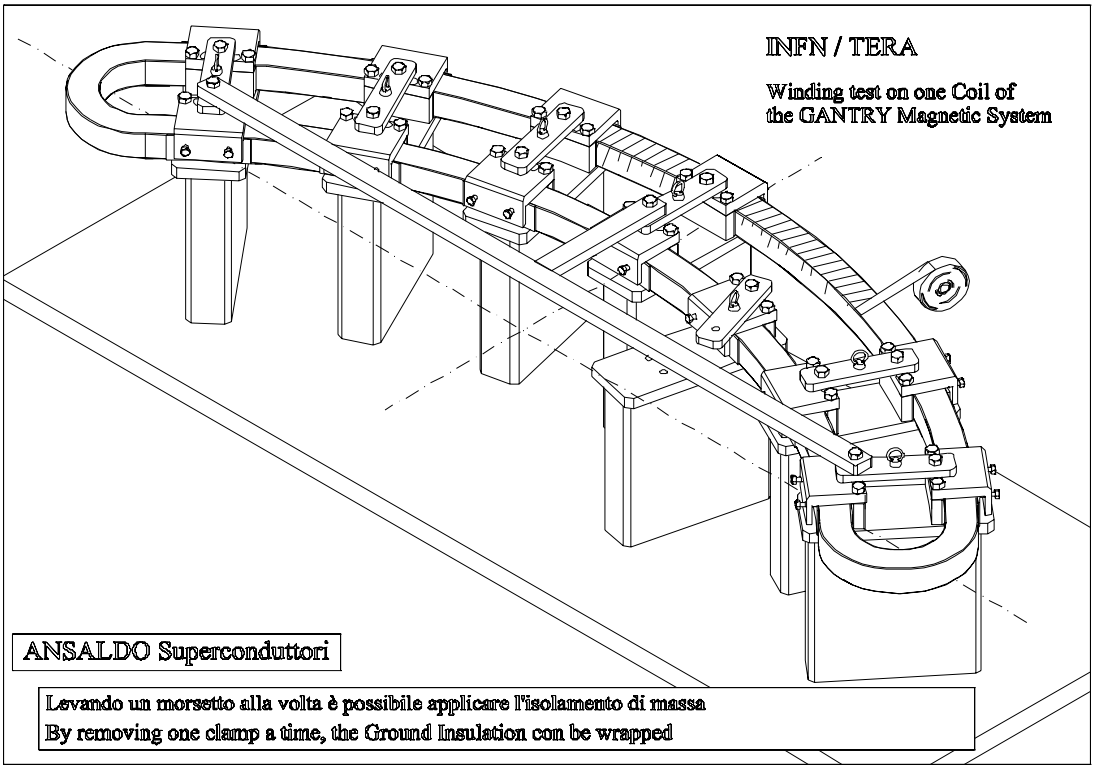

FIG. 35: Wrapping of the ground insulation.

Both clamps (point 5) and the plates (point 6) can be removed at any stage of the winding, to control the turn layout underneath.

Clamps, during the winding, are bolted down side up (fig. 30), to act as side containers only. Once the winding is completed, they are rotated by 180°, to clamp turns by means of two pressing bolts (fig. 31). All the 7 clamping sets of the coil in its final position can be disengaged from the winding platform (fig. 34). This is allowed because they are bolted on rectangular plates inserted into grooves machined on the winding platform. The two coil heads can be rotated by a key. Eventually an adjustable bolt could keep the head angular position. Figs 34 and 35 show the coil removed from the winding platform. A temporary "T" shaped stiffening structure helps keeping the overall coil shape. Once the coil has been removed from the winding platform and before to put it into the vacuum impregnation mould, the ground insulation is wrapped. By removing a clamp at a time a portion of the coil is accessible for the application of a tight wrap of dry glass tape. The quality, good application and proper thickness of the ground insulation are delicate design parameters. It acts as the interface with the mechanical supporting structure of the coil, and

it must ensure both the electrical strength (about which its thickness should be maximized) and a good thermal conduction through it, to allow an effective indirect cooling (about which its thickness should be minimized). The proposed way of applying the insulation improves the operational environment to perform and control that operation.

7.5 Final considerations

The proposed method for winding curved racetrack dipoles appears attractive, especially when using small conductors. Nevertheless, its feasibility has to be demonstrated through the construction of a coil full size mock-up. Ansaldo Superconduttori, basing on the above assumptions is now setting up an exhaustive winding test, that will foresee:

- the manufacturing of the coil form (done by INFN-Genova in their Workshop);
- the winding of one coil full size mock-up, whose dimension shall be full scale with respect the gantry magnetic system, and the number of turns and coil cross section ratio shall be decided in such a way to maximize the information obtainable from the test. It will be used a 5×3 mm^2 rectangular conductor, in pure aluminum, fully annealed and insulated with a half overlapped dry glass tape.
- the removal of the coil from the winding platform and the application of a continuous ground insulation.

8. MECHANICAL SUPPORTING STRUCTURE

The mechanical supporting structures have a fundamental importance, since the magnet is made basically of pure aluminum and therefore is not self-sustaining. We foresee to realize these structures by using an aluminum alloy. This material has a good thermal conductivity (a physical property of primary importance for the cooling), a relatively low density, and practically no ferro-magnetic properties. In the next future we will analyze several design solutions, taking into particular account the overall stresses acting onto the structure itself and the effect of the loads on the conductor insulation, which is the weakest structural component. In particular, the supporting structures will be designed in such a way to prevent the conductor to move: actually, even very small movements, of the order of 1 μm, may turn into a friction induced temperature increase in the conductor, which is sufficient to cause the magnet transition and then a loss of its superconducting properties.

Apart from the gravity, which should be considered only when designing the magnet suspension system, there are two main mechanical loads acting onto the supporting structures: the cooling forces and the Lorentz forces. The first load is due to the relative thermal contractions of the different materials composing the dipole. This load acts during the cooling down from room temperature to the operative temperature (4.5 K). In particular the aluminum alloy and the pure aluminum contract as 4.3‰, the insulation as 6 ‰ and the Rutherford cable as 2.6‰; these differences are large enough to generate not negligible stresses inside the winding. Moreover a thermal analysis in quasi-static conditions will be performed to determine the initial dimensions of winding and supporting structures (at room temperature), in such a way that their final values (at the operative temperature) would be equal to the designed ones.

The Lorentz forces, both in axial and in radial direction, determine the second load. While the Lorentz force in the axial direction is not dangerous, as it tends to compact the system by pushing one half of the magnet against the other one, the Lorentz force in the radial direction is much more critical. Actually, it acts as a repulsion force between the two arcs of every coil, in which the current flows in opposite directions. The Lorentz force oscillates during the magnet operation: if a very large number of oscillation cycles in the whole magnet life are foreseen, a fatigue analysis of the supporting structures has to be performed. On the contrary, a linear fracture mechanic analysis seems not to be required (unless accidental impact loads are to be considered). A fracture induced by transgranular cleavage is non likely to occur, thanks to the FCC crystalline structure of aluminum alloys: however, if particular thermal treatments should produce boundary precipitates (which may cause intergranular fracture) an impact test at the liquid nitrogen temperature is strongly recommended.

9. CRYOGENIC LAYOUT

The superconducting magnet is designed to operate between 4.5 K and 5.4 K (in any case below 6 K). It will be indirectly cooled through the aluminum alloy mechanical structure (thermal conductivity ≈0.1 W/cm K at 4.5 K) by means of cryocoolers, so that the use of cryogenic fluids will be avoided. The reasons of this choice are two: first, the design of a cryogenic vessel is complicated by the rotation and, second, the gantry will operate in a medical environment where a “cryogen free” magnet is preferred for a matter

of safety and because it does not need periodic refill. The Gifford-Mc Mahon cryocoolers, largely used for cryogen free systems, are preferred because they are simple to use and fairly reliable (12-18 month maintenance-free continuous operation).

The magnet will be partially charged and discharged during the clinical treatment, so it cannot work in persistent mode via a superconducting switch but has to be supplied continuously. As the current leads are always connected to the magnet giving the main contribute to the heat losses, they must end with HTCS bars working between 4.5 K and about 50 K. The first stage of the cryocoolers (T = 50 K) will be connected to the intermediate stage of the current leads (metal-superconductor interface) and to the thermal shields. Tab. IV shows the different contributes to the heat load P at 4.5 K and 50 K.

TAB. IV: Heat losses in steady state conditions.

	P @ T = 4.5 K (W)	P @ T = 50 K (W)
Radiation	<0.1	5
Conduction (tie rods and wires)	0.6	10
Current leads (at I_{max} = 1000 A) (at I = 0)	1.5 1.5	100 60
Total	**2.2**	**115**

It must be noted that, among the commercial cryocoolers, only one is reported to have 2.25 W cooling power at 4.2 K (supplied with 6.4 kW), so that the maximum heat load is limited by that value. Due both to this reason and to the fact that the current leads are the larger source of heat, the maximum current must be not higher than 1000 A. So, in normal operation, only one cryocooler is needed but during the magnet charge and discharge, as well as during the cool down, higher power is required (see next paragraph). To supply the additional power a second cryocooler is foreseen. The two cryocoolers will operate in parallel during both the transients and the magnet cooling or, alternately, in case of failure or maintenance of one of them. A single stage cryocooler operating at 50 K could be necessary to compensate the steady state heat load at 50 K mainly due to the heat conduction through the metal sections of the current leads.

9.1 AC losses

When the current of the bending dipole is changed, the field variation at the winding produces heat dissipations. We can identify the following mechanisms: 1) hysteretic losses in S/C filaments, 2) coupling losses in the multi-filamentary strand, 3) eddy currents in the conductor stabilizer.

In order to evaluate the losses, we have to refer to the coil-operating mode. We have considered a coil operation as follows:

- The starting bending field is 4 T.
- The field is decreased in step of 0.025 T. The time to reduce the field is 1 s.
- The field is kept constant for 1 s between two variations.
- Step by step, the field decreases down to a minimum of 3 T.

We will give three different values of the losses for each mechanism: a) The peak dissipation, in W, corresponding to the field step; b) The average dissipation, in W, c) The total release of energy, in J. We think that the latter is the most significant value, because it can be associated to an adiabatic increase of the coil temperature. In this case, the safety condition is that during the process the coil temperature is always less than the sharing temperature.

9.1.1 Hysteretic losses in filaments

With the aim to evaluate the hysteretic losses, we have to involve a well defined $J_c(B)$ curve. Typically, a Kim-Anderson behavior can be considered $J_c(B) = \frac{J_{c0} B_0}{B + B_0}$, where J_{c0} and B_0 are parameters depending on the conductor. Using the curve of Fig. 36, we find B_0=1 and J_{c0}= 1.58 10^{10} A/m^2.

Let a the filament diameter, the hysteretic losses for a close loop between fields B_1 and B_2 is:

$$Q_{12} = \int_{B_1}^{B_2} \frac{8}{3\pi} \frac{a\, J_{c0}}{1+B} dB = \frac{8}{3\pi} a\, J_{c0} \ln\left(\frac{1+B_2}{1+B_1}\right) \qquad (8)$$

When the bending field is B=4 T, the peak field at the winding is B_{2max} = 5.5 T. At B = 3 T B_{1max}= 4.13 T. The expression (8) must be modified taking into account the field distribution all over the winding. Supposing that the field B_2 ranges from 0 to B_{2max} (or

from 0 to B_{1max} for B_1) linearly in the winding, we have Q_{12}= 1.6 10^4 J/m^3. In half a cycle, in the total volume occupied by the superconductor (V_{sc}= 0.036 m^3), we have a total dissipation of 288 J. The transport current can increase this value of 1/3, so that we can assume a total dissipation of 374 J. The average power dissipation during the field variation (80 s) is 4.6 W.

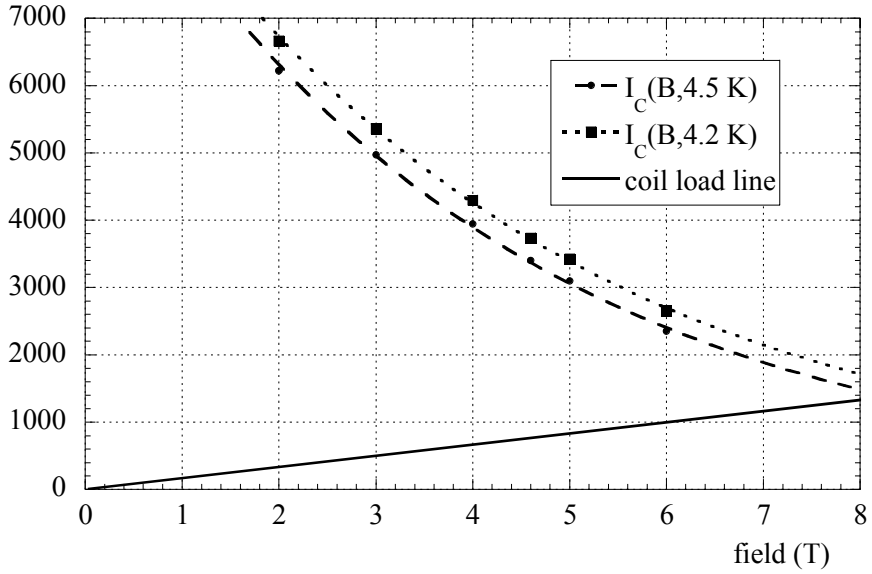

FIG. 36: I_c(B) characteristic with coil load line.

9.1.2 Coupling losses

The characteristic time constant for these losses is $\tau = \frac{\mu_0}{2\rho_e}\left(\frac{L}{2\pi}\right)^2$, where L is the twist pitch and ρ_e the transverse resistivity. Using L=0.02 m and ρ_e= 3.4 10^{-10} Ωm, we find τ=20 ms. Since the time constant is negligible compared with the rise time T=1 s, we can use for the coupling losses the relation $Q_c = \frac{2\Delta B^2}{\mu_0}\frac{\tau}{T}$= 17 J/m^3 per field step (when averaging the field at the winding). In the volume of the multi-filamentary strand (0.09 m^3), the total average dissipation is 0.75 W, the peak dissipation is 1.5 W and the total dissipation is 62 J.

9.1.3 Eddy currents

In our case we can use the formula $Q_e = \frac{\dot{B}^2}{12\rho_{Al}} d^2$, where ρ_{Al} the resistivity of pure aluminum ($6\ 10^{-11}$ Ωm at B=5÷6T) and d is the conductor dimension perpendicular to applied field (d=0.0032 m) per field step. We find a peak dissipation of Q_e=9 W/m^3 (then totally 4.5 W in the winding), and a total energy release of 180 J.

9.1.4 Temperature variation at the winding

The total energy release to ramp down the field from 4T to 3T in steps of 0.025 T is Q_{tot}= 616 J. Supposing that this energy is adiabatically deposited in the winding only, the temperature increases up to 5.8 K (i.e. less than the sharing temperature).

10. CONCLUSION

We are convinced that one ion gantry head of radius 160 cm can be realized using a superconducting magnet to give approximately 4 T with a cryocooler of 4.2 K. With respect to the available gantries proposed so far, it would allow a reduction of the weight of the cryostat (approximately 5.0 t totals with one cold mass of approximately 2.5 t) and, clearly, one could expect a not negligible cost reduction.

One of the main characteristics of the magnet superconductor for the gantry is in fact the lack of cryogenic liquids, which facilitates installation in hospital environment. The magnet in fact will be indirectly cooled by two stages cryogenerators connected to the mechanical structure. This choice is dictate by the necessity to maintain the thermal equilibrium to the lowest possible value and however not exceeding 2.5 W at 4.2 K (the maximum cooling power for commercial cryogenerators is of 3.0 W at 4.3 K).

In this study the beam optics and the particle tracking have been preliminary studied. These points are going to be deeply investigated in the following months and particular care will be devoted to integrate the SC dipole in the overall line design, from the synchrotron extraction to the patient. It has been also investigated the possibility to vary the magnetic field in the SC dipole to cope with an active scanning system in which the dose deposition in depth is varied changing the beam energy at the synchrotron extraction.

Industry, in the specific case Ansaldo Superconduttori s.p.a., is interested in the technological transfer in the specific and elitist field of the medical Physics with a product

of remarkable interest not only scientifically speaking, but also commercially thinking.

ACKNOLEDGEMENTS

The intellectual copyright of the present project is a joint property of INFN, ANSALDO Superconduttori and TERA Foundation. No use is permitted without permission of all institutes.

REFERENCES

(1) M. Pavlovic, private communication.

(2) Ch. Carli, Ch. Rocher, N. Fietier, M. Pinardi, EULIMA: Preliminary Design of the Gantry for the EULIMA Project, CERN, Geneva, Switzerland, March 1992.

(3) M. Pavlovic, Nucl. Instr. and Meth. **A399**, 439 (1997).

(4) L. G. Vorobiev, H. Wollnik, M. Winkler, GSI Report 97-06, April 1997.

(5) D. Budicin, M. Conte and V. Tamburini, TERA 95/9 FAS, June 1995.

(6) R. Orecchia, A. Zurlo, A. Loasses, M. Krengli, G. Tosi, S. Turrida, P. Zucali and U. Veronesi, European Journal of Cancer **34**, 456 (1998).

(7) R. Orecchia and M. Krengli, Tumouri **84**, 205 (1998).

(8) U. Amaldi, Nuclear Physics A **654**, 375c (1999).

(9) M. Pavlovic, NIM A **438**, 548 (1999).

(10) S. Reimoser, M. Pavlovic, NIM A **456**, 390 (2001).

(11) P.J. Bryant, Proton-ion medical machine study (PIMMS), Part I, CERN PS 99-010 (DI), 1999.

(12) P.J. Bryant, WinAGILE, http://nicewww.cern.ch/~bryant.

(13) ANSYS®, Revision 5.7, Swanson Analysis Systems, Inc.

(14) OPERA®, Version 7.5, Vector Fields Limited.